

Available online at www.sciencedirect.com

jmr&t
Journal of Materials Research and Technology
journal homepage: www.elsevier.com/locate/jmrt



Review Article

Additive manufacturing of structural ceramics: a historical perspective



Joshua S. Pelz^{a,b}, Nicholas Ku^b, Marc A. Meyers^a,
Lionel R. Vargas-Gonzalez^{b,*}

^a University of California, San Diego, La Jolla, CA, 92093, USA

^b United States Army Research Laboratory, Weapons and Materials Research Directorate, Aberdeen Proving Ground, Aberdeen, MD, 21005, USA

ARTICLE INFO

Article history:

Received 25 March 2021

Accepted 30 July 2021

Available online 11 August 2021

Keywords:

Additive manufacturing

Rapid prototyping

3D printing

Ceramics

Stereolithography

Robocasting

ABSTRACT

Additive manufacturing (AM) has created a new era of digital manufacturing, where engineering practices, computer-aided design platforms, and part sourcing pipelines are dramatically changing. AM techniques are capable of producing plastic, metal, and ceramic components for both prototyping and end-use purposes. In this review, the fabrication of dense, structural advanced ceramic components using the seven families of additive manufacturing is discussed through a historical perspective. Initial studies on additive manufacturing of ceramic materials were reported just a few years after those of metal and plastic materials. However, industrial application of ceramic additive manufacturing is more than a decade behind metallic and plastic materials. Many of the challenges of ceramic AM can be traced back to the intrinsic difficulties of processing structural ceramic materials, including high processing temperatures, defect-sensitive mechanical properties, and poor machining characteristics. To mature the field of ceramic AM, future research and development should focus on expanding material selection, improving printing and post-processing control, realizing single-step processing, and unique capabilities such as multi-material and hybrid processing.

Published by Elsevier B.V. This is an open access article under the CC BY-NC-ND license (<http://creativecommons.org/licenses/by-nc-nd/4.0/>).

Abbreviations: AM, Additive manufacturing; UV, ultraviolet; SLS, selective laser sintering; FDM, fused deposition modeling; MIT, Massachusetts Institute of Technology; LCD, liquid-crystal display; DLP, digital light processing; DMD, digital micromirror device; LED, light-emitting diode; PDC, polymer derived ceramic; PBF, powder bed fusion; SLM, selective laser melting; IED, input energy density; PI, pressure infiltration; WIP, warm isostatic pressing; 3DP, 3D Printing; RB, reaction bonded; LOM, layered object manufacturing; FDC, fused deposition of ceramics; MJS, multiphase jet solidification; FEA, finite element analysis; DED, directed energy deposition; LENS, laser engineered net shaping; SALD, selective area laser deposition; SALDVI, selective area laser deposition vapor infiltration; 2PL, two-photo lithography.

* Corresponding author.

E-mail address: lionel.r.vargas-gonzalez.civ@mail.mil (L.R. Vargas-Gonzalez).

<https://doi.org/10.1016/j.jmrt.2021.07.155>

2238-7854/Published by Elsevier B.V. This is an open access article under the CC BY-NC-ND license (<http://creativecommons.org/licenses/by-nc-nd/4.0/>).

1. Introduction

1.1. Preface

In this review, we detail the history, recent advances, and future directions for additive manufacturing (AM) of bulk, dense structural ceramics. Advanced ceramics are attractive for use in structural applications due to their high hardness, wear resistance, and corrosion resistance. To achieve these properties, a relative density greater than 95% is necessary for structural ceramics, with many applications such as armor ceramics requiring above 98% relative density [1]. High hardness and wear resistance properties complicate machining processes; ceramic AM research is driven by the need for cost effective methods to manufacture complex components. Through our historical analysis of the development of ceramic AM, seminal works are highlighted to provide context for the lag in technology for ceramic AM compared with plastic and metal AM.

For readers interested in components with designed porosity such as lattice structures, several excellent reviews exist [2–4]. Specific applications for designed porosity include printing hydroxyapatite implants [5], bone scaffolds [6], and variable stiffness ceramic foams [7]. Bae [8] reviewed and investigated the use of direct ceramic casting using vat photopolymerization to create ceramic investment casting molds for applications like turbine blades with integrated cooling channels. Although the use of ceramic AM for creating molds is important, it is out of scope for this review. Several groups have used the additive manufacturing technique of direct energy deposition to develop ceramic coatings on titanium [9,10] and steel [11,12] to increase wear and corrosion resistance. Properties such as biocompatibility can also be improved by deposition of ceramic coatings [13]. Although this is an important body of research, coatings are also out of scope for this review.

1.2. Advanced ceramics and their applications

Advanced ceramics are characterized by exceptional wear, corrosion, and temperature resistance. These materials can be biocompatible, electrically activated, and optically active. Applications span nearly every industry, with an emphasis in the aerospace, automotive, defense, medical, and energy sectors. Engine components, body and vehicle armor, and load-bearing medical implants all rely on dense, structural advanced ceramics [14].

Ceramic forming is a mature technology with several methodologies at a commercial manufacturing scale, e.g. pressing, extrusion, slip casting, tape casting, gel casting, and injection molding [15]. However, these traditional forming techniques often only allow two-dimensional design freedom, cannot create internal or multi-scaled features, and require complicated and expensive dies [16]. In addition, engineering of chemically heterogeneous structures is limited due to the stochastic nature of traditional powder mixing and processing. Tape casting, without secondary layering steps, only allows control of the sheet thickness. Pressing and extrusion produce parts of simple geometry such as disks, rods, and tubes [17]. Slip casting [18], gel casting [19,20], and injection

molding [21] afford the most geometric freedom, but do not enable material heterogeneity. With the exception of layered tape-cast specimens, where layers may be of different materials [22], these techniques all produce chemically homogeneous parts. Furthermore, due to the exceptional wear resistance of advanced ceramics, machining is time consuming and expensive. In fact, machining of dense advanced ceramic parts can amount to more than 80% of the production cost [23].

1.3. Additive manufacturing

Additive manufacturing (AM), conversely, enables the production of parts with complex, multi-scaled geometries including internal structures [16,24,25]. Additionally, multi-material AM allows for tailored material heterogeneity by discrete layers and composition gradients [26–28]. The ISO/ASTM standard 52900:2015(E) defines the fundamental principle of AM processes as, “forming three dimensional parts by the successive addition of material” [29]. The primary distinction between additive processes is the method of joining, which establishes seven families of AM technologies: vat photopolymerization, powder bed fusion, binder jetting, material jetting, sheet lamination, material extrusion, and directed energy deposition [29]. These processes are described in Table 1, with information including material selection, special features, advantages and disadvantages, and mechanical properties and microstructure. AM is achieved in either a single-step process (commonly called ‘direct’) or multi-step process (commonly called ‘indirect’) [29]. Fig. 1 illustrates the difference between direct processes that simultaneously produce a desired shape with final properties and indirect processes that require two or more steps to produce the desired geometry with final properties. Metallic, ceramic, and polymeric materials have all been adapted for use in these AM processes, enabling the production of both prototypes and end-use components [14].

Additive manufacturing is best suited for low-volume production of complex geometries, because time and cost are weakly dependent on complexity; for masked AM processes, time and cost are fully-independent from complexity in the build plane [30]. A case study performed by Atzeni et al. [31] compared the cost of manufacturing an aluminum aerospace component using high-pressure die casting and powder bed fusion processes. Production volumes below 42 parts favor the AM powder bed fusion process, due to the high cost and long manufacturing time of the die. Further, AM affords the ability to make complex geometries that are impossible to create through subtractive manufacturing or forming processes.

It is important to note that mechanical properties are largely anisotropic for parts produced by AM, due to the layer-wise nature of the process [14]. In fact, the term ‘3D printing’ is a misnomer, as printing is a one- or two-dimensional process repeated layer-wise in the build direction. For this reason, mechanical properties will differ depending on the testing orientation with respect to the build direction. Anisotropic mechanical properties arise from differences between inter-layer and inter-trace bonding strength, microstructure texturing, and other printing artifacts [32].

1.4. Challenges in ceramic additive manufacturing

The commercial use of additive manufacturing to produce ceramic components is more than a decade behind that of polymeric and metallic materials. In addition, the adaptation of AM for ceramic materials occurred nine years after that of polymers [33]. This lag in technology is primarily due to the difficult processing conditions and quality requirements intrinsic to ceramic materials. For example, the lower melting temperatures of metallic and polymeric materials enables direct AM, wherein feedstock material is processed above its melting point, bonds to nearby material, and cools to maintain its desired shape with final properties, all within a single machine. In contrast, a majority of ceramic AM processes are indirect, wherein a green body is formed by the 3D printer using a binding agent to hold ceramic particles together and then several post-processing steps are required to attain final properties [34].

Post-processing steps include pyrolysis (up to 700 °C) and sintering (up to 2300 °C), which are necessary to remove binders from the green body and consolidate the ceramic powder into its final geometry with final properties. Green bodies formed by AM machines contain, at a maximum, 65–72 vol.% ceramic powder [34]. Post-processing to full density will result in dimensional shrinkage exceeding 30% [35], which can lead to warping, cracking, and poor dimensional control.

The mechanical properties of ceramic materials are defect-dominated due to their brittle nature and low damage tolerance. The hardness of alumina increases by more than 30% for a change in relative density from 92% to 98% [36]. This correlation between mechanical properties and flaw content dramatically increases the necessity of accurate processing control. Unfortunately, limited standardization exists for material feedstock production, process parameters, and post-processing, which leads to poor quality control in additive manufacturing processes [37].

2. The history of additive manufacturing

2.1. First attempts

The inception of additive manufacturing goes back to 1980 when Hideo Kodama [38], of the Nagoya Municipal Industrial Research Institute of Japan, invented the vat photopolymerization process and filed a patent for a “stereoscopic figure drawing device”. Kodama [39] developed a rapid, low-cost, and automated process for selectively curing liquid photo-hardening polymer using ultraviolet (UV) energy. Selective curing was accomplished by either a mask pattern or point-by-point using a laser, and repeated layer-by-layer to build a three-dimensional part. Although this work marks the first published record of a successful additive manufacturing process, it did not generate any commercial traction and Kodama's patent expired without proceeding past the examination stage.

In 1984, Charles Hull [40] patented and commercialized the first AM technology. He developed an “apparatus for

production of three-dimensional parts by stereolithography,” which was named SLA-1 [41]. In addition to inventing the machine and method, he created the STL (an abbreviation of stereolithography) file format to store geometric data for parts. This machine falls into the vat photopolymerization family of AM technologies. Hull [40] developed the SLA-1 with the intent of more efficiently producing prototypes. Closely following Hull's patent, the selective laser sintering (SLS) process, a type of powder bed fusion, was patented in 1986 by Deckard et al. [42]. They formed the company DMT based on their SLS technology, which was later acquired by 3D Systems. In 1987, Masters [43] patented a process for ejecting particles or droplets or using a laser to attract material to a specific point to automatically create three-dimensional objects. Masters' patent covers both material jetting and direct energy deposition processes. The following year, the sheet lamination process was patented by Feygin [44] with the company Helisys. Woven fiber composites impregnated with a bonding agent were initially used as feedstock material to build 3D parts with the sheet lamination method [45]. In 1989, two additional patents were filed that covered fused deposition modeling (FDM) [46], a type of material extrusion, and 3D Printing [47], the copyrighted name for binder jetting. Crump [46] started the company Stratasys based on FDM, while Sachs et al. [47] invented the binder jetting process at the Massachusetts Institute of Technology (MIT) and then licensed their technology to several companies. A timeline of the patents and first published accounts with a ceramic feedstock is shown in Fig. 2.

2.2. Rapid prototyping to additive manufacturing

These processes, then termed rapid prototyping techniques, were first surveyed in 1991 by Kruth [48]. In their infancy, additive manufacturing techniques were believed to be solely useful for prototyping. However, during the 1990s few new processes were developed and instead an effort was made to move towards higher process efficiency and production of end-use parts [49]. Indeed, the term ‘additive manufacturing’ had already begun to replace ‘rapid prototyping’. Six-fold and eight-fold decreases in process time for vat photopolymerization and material extrusion, respectively, were realized during the 1990s [49]. This decrease in processing time enabled a new wave of rapid throughput manufacturing, where one-off parts could be ordered, manufactured, and shipped in under 24 h [50].

Even more importantly, however, was the rapid expansion of materials amenable for additive manufacturing processes: high performance polymers, metals, and ceramics enabled the development of functional, end-use parts. AM has great potential for creating composite parts with graded compositions, where virtually any powder material can be combined and printed into heterogeneous components with spatially tailored properties [51]. This trend continues currently, where the major goals of AM research include the development of quality control mechanisms and expanding the AM material library to facilitate the production of end-use parts [52]. Today, major players in the ceramic AM commercial sector produce

Table 1 – The seven families of AM processes described for structural ceramic components. Material selection, special features, advantages, disadvantages, multi-material capability, and mechanical properties and microstructure are summarized for each ceramic AM technique.

Classification	Technique	Direct/ Indirect	Description	Feedstock Material	Minimum Required Binder Content [vol.%]	Minimum Feature Size [μm]	Maximum Density [% TD]	Average Flexural Strength [MPa]	Multi- material Capable	Challenges	Advantages
Vat Photo- polymerization	SL	Indirect	Stereolithography uses a laser to cure resin point-by-point.	Liquid vat of photocurable resin loaded with ceramic powder.	40 [61]	102 (x-y); 25 (z) [61]	97 (Al ₂ O ₃) [61]	275 (Al ₂ O ₃) [61]	No	Limited material selection (refractive index issues prevent the use of many borides, carbides, and nitrides);	Fast printing time; highest resolution; good surface finish; large part size
	DLP	Indirect	Digital light processing uses a light projector to selectively cure resin layer-by-layer.		55 [66]	40 (x-y); 25 (z) [66]	99.3 (Al ₂ O ₃) [64]	427 (Al ₂ O ₃) [64]	No		
Powder Bed Fusion	SLS	Indirect	Selective laser sintering uses a laser to partially fuse or sinter ceramic powder point-by-point.	Ceramic powder bed; may contain a polymer binder.	10 [83]	200 (x-y) [83]	89 (Al ₂ O ₃) [82]	148 (Al ₂ O ₃) [82]	No	Poor surface finish; low green body density	Overhangs are supported; wide material selection; good resolution
	SLM	Direct	Selective laser melting uses a laser to fully sinter or melt ceramic powder point-by-point.	Ceramic powder bed	0 [79]	100 (x-y); 100 (z) [79]	100 (Al ₂ O ₃) [80]	500 (Al ₂ O ₃) [80]	No	Severe thermal gradients cause part failure and limit size	
Binder Jetting	3DP	Indirect	Three-Dimensional Printing uses an inkjet head to selectively deposit liquid binder to fuse ceramic powder	Ceramic powder bed	60 [100]	50 (x-y); 95 (z) [33]	98.5 (ZTA) [98]	441 (ZTA) [98]	No	Poor surface finish; low green body density	
Material Jetting	MJ	Indirect	Material jetting uses a inkjet head to rapidly eject droplets of photocurable or thermoplastic resin loaded with ceramic powder. Solidification happens by cooling or UV lamp curing.	Thermopolymer or photocurable ink loaded with ceramic powder	65 [109]	20 (x-y); 10 (z) [106]	99 (PZT) [109]	Not reported	Yes	Low green body density	High resolution; multi-material capable

(continued on next page)

Table 1 – (continued)

Classification	Technique	Direct/ Indirect	Description	Feedstock Material	Minimum Required Binder Content [vol.%]	Minimum Feature Size [μm]	Maximum Density [% TD]	Average Flexural Strength [MPa]	Multi- material Capable	Challenges	Advantages
Sheet Lamination	LOM	Indirect	Layered object manufacturing uses a laser to cut two-dimensional profiles from a ceramic green tape, which are layered and fused through pressure and heat.	Tape cast polymer sheets loaded with ceramic powder	44 [118]	190 (z) [118]	97 (Si_3N_4) [118]	700 (Si_3N_4) [118]	Yes, but only layer to layer	Defects and poor bonding at layer interfaces	Highest speed; layered composites
Material Extrusion	DW	Indirect	Direct write techniques extrude a ceramic slurry, point-by-point, that solidifies via rheological, temperature, or photocurable effects.	Slurry of ceramic powder, solvent, and binder	<10 [137]	1000 (x-y); 850 (z) [137]	98 (Al_2O_3) [137]	145.5 (Al_2O_3) [137]	Yes	poor resolution; difficult feedstock design	Low-cost process; multi-material capable; near-net shaping
	FDC	Indirect	Fused deposition of ceramics extrudes thermoplastic filament loaded with ceramic powder from a heated nozzle, point-by-point.	Thermopolymer filament loaded with ceramic powder	45 [136]	250 (x-y); 254 (z) [136]	>99 (Si_3N_4) [136]	908 (Si_3N_4) [136]	Yes	It is difficult to load filament with enough ceramic powder to facilitate full densification	low-cost process; multi-material capable
Directed Energy Deposition	LENS	Direct	Laser engineered net shaping uses a high-powered laser to melt a jet of powder point-by-point in a process similar to welding.	Ceramic powder	0 [152]	400 (x-y); 500 (z) [152]	98 (Al_2O_3) [145]	Not reported	Yes	Severe thermal gradients cause part failure and limit size	direct processing; multi-material capable

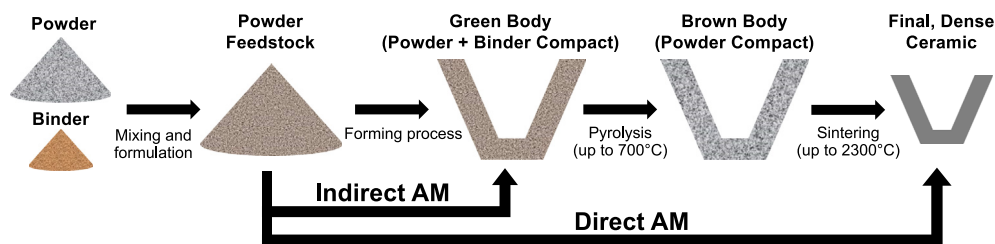


Fig. 1 – Direct additive manufacturing processes simultaneously produce a desired shape with final properties, whereas indirect processes require two or more steps to produce the desired geometry with final properties. For ceramic materials, pyrolysis and sintering are necessary to attain final properties after an indirect process is used to form a green body.

end-use components for medical, aerospace, defense, automotive, and energy applications [53].

3. Vat photopolymerization for advanced ceramics

3.1. Foundations

Vat photopolymerization, originally called stereolithography, was the first family of additive manufacturing processes adopted for commercial use. 3D Systems dominated the market with their SLA-250 machines [41], an industrial iteration on their SLA-1 prototype machine. Three-dimensional parts are produced layer-by-layer, by the selective application of UV energy to photocurable resin, as illustrated in Fig. 3A. In order to print ceramic parts, ceramic powder is loaded into the resin [54]. Resin can be cured point-by-point using a laser or layer-by-layer using a light projector or masked liquid-crystal display (LCD) screen. Processes where the entire layer is cured simultaneously can reduce build times by a factor of 100 [49]. This AM technique excels at producing highly complex geometries with fine resolution and good surface finish. Vat photopolymerization can be carried out in either a bottom-up or a top-down approach [48]. The bottom-up approach has the advantage that uncured resin

will drain back into the vat, reducing the volume of resin necessary to build a part [52]. Vat photopolymerization is an indirect process for ceramic materials because the photocurable resin, which is essential to the polymerization process, must be removed through post-processing steps to obtain a dense ceramic component.

3.2. Evolution

In 1995, Griffith and Halloran [55] first demonstrated the use of vat photopolymerization for fabrication of ceramic parts, with the goal of more rapidly producing metal casting molds. Vat photopolymerization was studied for silica, alumina, and silicon nitride particulate loaded resins. Major challenges were the cure depth and rheology of the ceramic loaded resins. Viscosity increases exponentially with volume fraction ceramic material, which competes with the requirement that the resin must be able to flow across the build surface. The three main factors found to determine cure depth were particle size, interparticle spacing, and refractive index difference between the resin and ceramic particles, with refractive index difference as the dominant factor [56]. Alumina and silica were both cured at depths of hundreds of micrometers, but silicon nitride could only be cured to tens of micrometers due to its large refractive index difference from the diacrylate resin. Silicon nitride parts could not be produced due to the

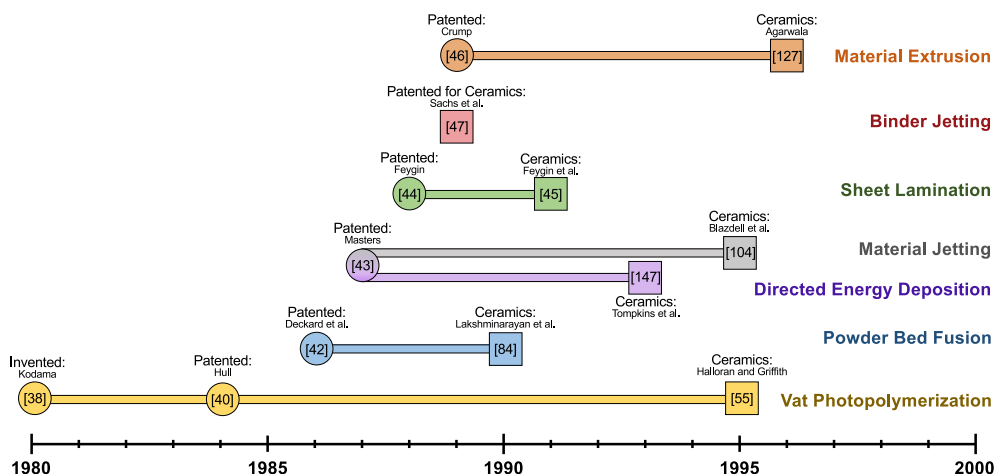


Fig. 2 – The invention of additive manufacturing processes occurred in the 1980s, but the adaptation of these techniques for ceramic materials extended into the 1990s. The time between invention and ceramic material use varied greatly, with binder jetting being invented using ceramic materials versus vat photopolymerization which was invented 15 years before ceramic materials were successfully demonstrated.

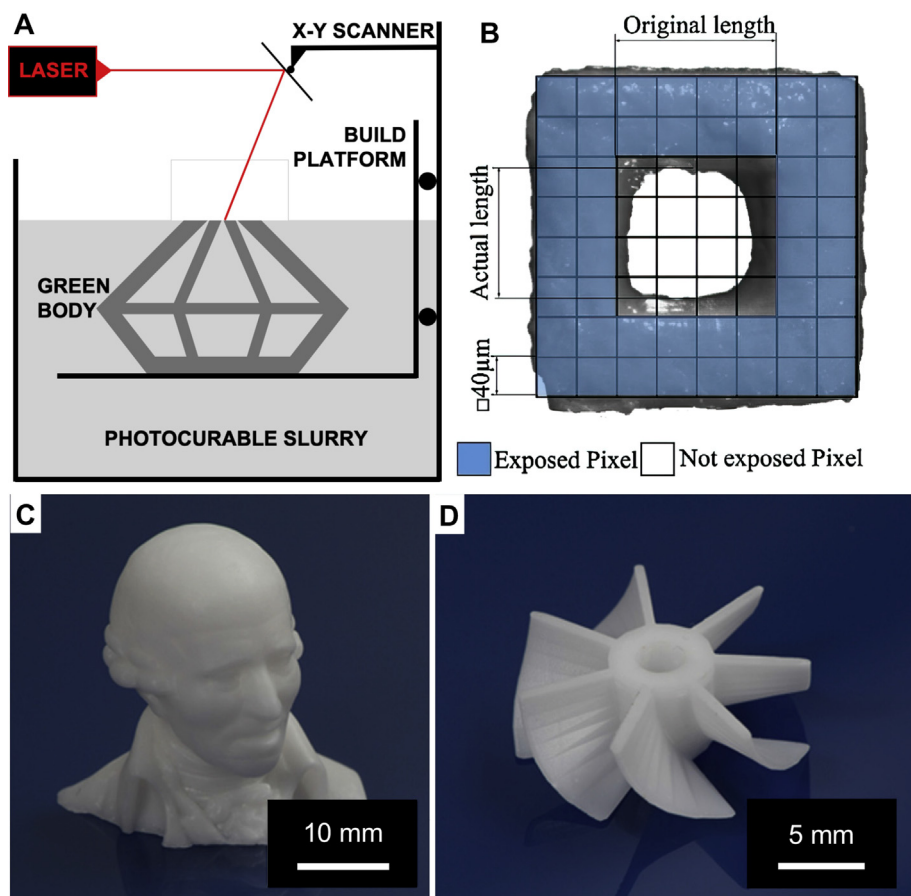


Fig. 3 – (A) Diagram illustrating the vat photopolymerization technique, where three-dimensional parts are created by selectively curing a photocurable resin layer-by-layer. (B) Overexposure occurs due to light scattering in highly loaded particulate suspensions [61]. (C,D) Dense zirconia specimens with complex geometry were produced with no visible layer interfaces after post-processing [61].

low cure depth. Alumina parts were produced from 40 vol.% alumina powder (average particle size of $0.34\ \mu\text{m}$) in diacrylate resin with dimensional stability in both thick and thin sections. Due to light scattering, parts showed 5–15% dimensional errors. Sintering at $1550\ ^\circ\text{C}$ resulted in 100% relative density and fracture surfaces free of printing artifacts such as layer lines [57].

Two years later, Griffith and Halloran [58] conducted a thorough follow-up study on the effects of laser parameters with the goal of predicting and improving the cure depth for many advanced ceramics, including TiO_2 , SiC , Si_3N_4 , and Al_2O_3 . Cure depths were modeled for 40–50 vol.% ceramic particulate loaded resin. Cure depth can be modeled using a Beer's law equation combined with an extinction coefficient,

$$D_c = \frac{2\langle d \rangle}{3Q} \frac{n_0^2}{\Delta n^2} \ln\left(\frac{E_0}{E_{\text{crit}}}\right), \quad (1)$$

where d is average particle size, Q is the scattering efficiency term, Δn^2 is the squared refractive index difference between the ceramic and photocurable monomer, and E_0 is the energy density [58]. The refractive index difference between the ceramic and resin was, again, found to have the greatest effect on cure depth, followed by interparticle spacing, and lastly

(less important than previously thought) ceramic particle size. Although particle size has a minor effect for cure depth, it significantly impacts slurry rheology and post-processing characteristics, and must be carefully controlled. For highly-loaded colloidal alumina and silica suspensions, Garg et al. [59] studied light adsorption differences between short-pulse and constant light sources. Relationships were experimentally verified and, in agreement with previous work, interparticle spacing has an important effect.

In 1998, Hinczewski et al. [60] determined that heating the vat of photocurable suspension will significantly reduce viscosity, which enables higher ceramic content. For an alumina-diacrylate photocurable suspension, viscosity was reduced by a factor of six as temperature was increased from 25 to $70\ ^\circ\text{C}$. This novel method enabled an unusually high ceramic content of 53 vol.%, while maintaining acceptable rheological (less than $5\ \text{Pa}\cdot\text{s}$) and cure-depth (greater than $200\ \mu\text{m}$) properties for printing.

3.3. Recent developments

Challenges faced in early vat photopolymerization studies of ceramic materials, including suspension rheology,

particulate-induced light scattering, and low cure depth, remain a major focus in recent studies [54]. The requirement for feedstock material with high ceramic content leads to rheological challenges, scattering, and low cure depth. With the goal of eliminating rheological challenges, Chartier et al. [61] used a novel processing approach in 2002 that enabled the use of photocurable suspensions with ceramic content up to 60 vol.%. Instead of relying on fluid flow to recoat the build surface, the photocurable alumina suspension was dispensed using a piston and spread in even layers using a doctor-blade. This method enabled the printing of uniform layers down to 25 μm . An added benefit of tape-casting feedstock material for the vat photopolymerization method is that over-hang structures are supported, and shrinkage, warping, and cracking are reduced. Alumina (average particle size of 1.5 μm) parts sintered at 1700 °C achieved relative densities of 97% and had flexural strengths of 275 MPa, comparable to those of traditionally processed specimens (250–350 MPa). Zhang et al. [62] added fine grains and sintering additives to improve the densification of parts printed from large particle-size alumina powder. For a ceramic content of 50 vol.%, alumina (average particle size of 10.34 μm) parts sintered at 1600 °C showed minimal densification. By using a bimodal mixture of alumina powder with average particle sizes of 10.34 (85%) and 1.05 μm (15%), in addition to 1 wt.% MgO and 3 wt.% TiO₂, a relative density of 92.97% was achieved. While a relative density of 93% is insufficient for structural ceramic components, this study demonstrates the potential of low-cost feedstock powders combined with fine grains and sintering additives. For printed zirconia parts, adding 7.5 vol.% 3Y-TZP increased the relative density from 91.84% to 96.40% [63].

In the mid-2010s Schwentenwein et al. [64] and Scheithauer et al. [65] used a masked, bottom-up approach, termed digital light processing (DLP), to improve the resolution and processing speed for alumina parts. During the build process, a part is submerged into the vat of photocurable suspension with the build surface just 25 μm from the bottom of the vat. The entire layer is then cured at the same time using a digital micromirror device (DMD) based on light-emitting diodes (LED). Build-up speeds less than 30 s per layer, irrespective of layer complexity or selected area, were achieved through the dynamic masked curing process. Mitterramskogler et al. [66] utilized different light curing strategies to reduce printing flaws and improve densification. Overexposure, where material outside of selected pixels is cured, is caused by light scattering and is shown in Fig. 3B. Constant, exponential, and softstart light curing strategies, which change light intensity with respect to time during curing, were tested by pulsing the DMD at a specified duty-cycle. The softstart strategy starts curing at a low intensity (duty-cycle near 10%) and then steps up to full intensity (duty-cycle of 100%). No significant change was observed for exponential curing as compared to constant curing. Conversely, softstart curing reduced cracks and increased green density. A second strategy, using a cure depth greater than the layer height, was shown to improve inter-layer bonding. For a layer height of 25 μm , cure depth of 150 μm , and softstart curing strategy, dense zirconia specimens were produced with no visible layer interfaces after post-processing (Fig. 3C, D).

Ding et al. [67] fabricated SiC green bodies using vat photopolymerization in 2019, a major accomplishment because the high absorbance of SiC and high refractive index difference between SiC and photocurable resin. The refractive indices for diacrylate monomer, Al₂O₃, Si₃N₄, and SiC are 1.46, 1.70, 2.10, and 2.65, respectively. A large refractive index difference and absorbance results in a low cure depth, which impedes vat photopolymerization processing. This phenomenon was initially reported on by Griffith and Halloran [58], and fabrication of parts using Si₃N₄ and SiC suspensions was not achieved. Ding et al. [67] achieved a cure depth of 60 μm by using large SiC particulates of diameter 15 μm and a ceramic content of 40 vol.%. Cure depth was increased to 66.8 μm by adding 1 wt.% nanometer-sized SiC powder [68]. The nanometer-sized SiC powder also improved suspension stability, which enabled fabrication of complex SiC green bodies. However, neither the post-processing characteristics, sintered density, nor mechanical performance of these parts was reported on; low ceramic content and large particle size will hinder densification during sintering. In a subsequent study, Ding et al. [69] printed small-scale (<5 cm) SiC mirrors for potential aerospace applications. Photocurable suspensions contained 45 vol.% ceramic content, consisting of 1 wt.% alumina (sintering additive), 1 wt.% nanometer-sized SiC powder, and remainder micrometer-sized SiC powder. Sintering at 1800 °C resulted in a relative density of 85.2% and flexural strength of 78.6 MPa. To increase structural performance, polycarbosilane was infiltrated into the sintered parts and then pyrolyzed at 1200 °C. After eight cycles, a relative density of 93.5% and flexural strength of 165.2 MPa was achieved.

A notable alternative to loading ceramic particles into photocurable resins is the polymer derived ceramic (PDC) method. In this approach, photocurable preceramic resins are formed through vat photopolymerization and then pyrolyzed at temperatures 1000–1300 °C to derive ceramic parts with final properties [70]. Significant energy savings are realized by using these relatively low post-processing temperatures, as compared to traditional ceramic sintering temperatures. In addition, this method enables the production of ceramic parts with excellent surface finish. One major advantage is that carbides, borides, and nitrides can all be derived from preceramic resins [71]; these materials are challenging to cure using traditional ceramic particle loaded resins due to their large refractive index differences and high absorbance values. A variety of ceramic materials can be produced by varying the preceramic feedstock, including SiOC using siloxane-based polymers, SiOCN by combining siloxanes with silazanes, and SiC by adding silane-based polymers [72]. An initial study by Eckel et al. [73] from HRL Laboratories demonstrated the feasibility to produce dense SiOC microlattices that outperform ceramic foams with respect to shear and compressive strength. In 2020, O'Masta et al. [74] used the PDC method in combination with reinforcement particles (mullite, alumina, and silicon nitride) and whiskers (SiC) to produce ceramic matrix composites with improved toughness. The addition of SiC whiskers to the SiOC matrix increased toughness by a factor of three. Guo et al. [75] demonstrated an additional benefit of the PDC method, wherein elastomeric material can be printed, stretched/deformed, and then pyrolyzed into

ceramic lattices with unique geometries that may be difficult to print in a single orientation. The main drawback of the PDC approach is shrinkage-induced cracking and pore formation during pyrolysis, which imposes limits to the maximum thickness of structures. Thus, this method shows significant promise for lattice structures with strut diameters below approximately one millimeter but will face challenges for structural applications that require dense, bulk ceramic components.

The PDC method is not limited to vat photopolymerization processes, and has been demonstrated for powder bed fusion [source], binder jetting [source], material jetting [source], material extrusion [76].

4. Powder bed fusion for advanced ceramics

4.1. Foundations

The powder bed fusion (PBF) process, originally called selective laser sintering (SLS) or selective laser melting (SLM), produces three-dimensional parts by fusing powder via selective application of laser energy in a layer-by-layer process, as shown in Fig. 4A. This process is unique in that it can be a direct or indirect ceramic AM process. If a high-power laser is used that can melt or fully-sinter the ceramic powder, a dense part with final properties is directly created and no further processing necessary. Conversely, if the laser only partially melts or joins powder, post-processing steps are required to attain final properties. PBF, like other powder bed processes, has the advantage that overhangs are supported by unbound powder, which is removed in post-processing steps. The application of PBF for structural ceramics has seen limited success because green bodies have low relative densities. One potential method for improving final sintered density is isostatic pressing of printed green bodies prior to pyrolysis and sintering [77]. Other challenges include poor surface finish and thermal-gradient induced cracking, which restricts geometry and overall dimensions.

4.2. Evolution

Original powder bed fusion methods used for advanced ceramics required the ceramic powder to be coated in a thin

polymer layer, which is melted by the laser beam to selectively bond powder together into a green body [78]. Post-processing, namely binder removal and sintering, was therefore required to produce the final part. Relatively few publications [79–81] cite successful fabrication of dense ceramic parts using a single step PBF process, because thermal shock causes part failure and is intrinsic to the rapid heating and cooling cycle of creating a melt pool. Thus, many approaches create porous scaffolds, which are subsequently infiltrated with molten polymeric or metallic material. This process produces composite parts with improved toughness. In order to reduce thermal-shock-induced cracking, each powder layer can be pre-heated, which decreases the temperature differential between unbound powder and the melt-pool [82]. An additional complication of PBF of ceramic materials is their low density relative to metallic powders, which further hinders the flowability of fine ceramic powders. To address this issue, Mapar et al. [83] used spray-drying to increase the flowability of fine powders (1–5 μm) by creating larger agglomerates with 30 μm diameter.

Lakshminarayan et al. [84] performed the first powder bed fusion study for ceramic materials in 1990. Alumina parts were produced through an indirect process, where an alumina-ammonium phosphate powder mixture was used. During laser irradiation, the ammonium phosphate powder melts and forms a glassy phase around the alumina particles. Ammonium phosphate has a melting point of just 190 $^{\circ}\text{C}$, which significantly reduces the laser power required. Complex shaped parts were produced but showed poor dimensional tolerance, surface finish, and mechanical properties due to high porosity.

A different indirect approach used by Vail et al. [85] in the following year employed polymer coatings as intermediate binders for printing soda-lime glass parts. Glass powder was mixed with polymer and spray dried through the centrifugal atomization method. Parts fabricated using coated powders had improved edge definition and stability compared to those created from a powder-polymer mixture. A similar trend was observed by Subramanian et al. [78], where green parts built from binder-coated powder showed flexural strengths twice that of mixed systems. The flexural strength of green parts increases with energy density up to a point, followed by a reduction in strength as polymer degradation occurs. Therefore, short scan vectors are optimal for increasing green strength, while avoiding polymer degradation. Further, green

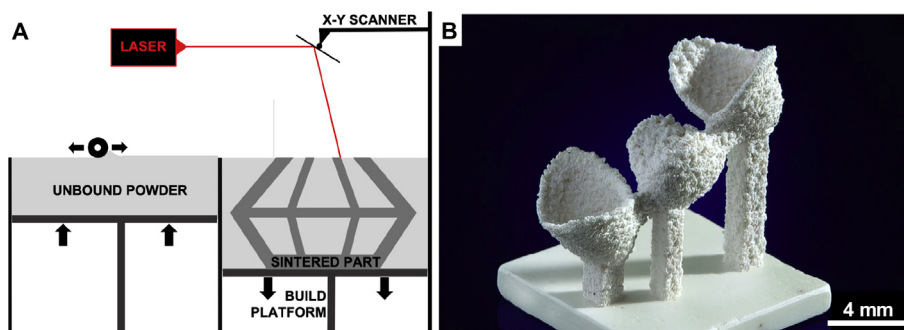


Fig. 4 – (A) Diagram illustrating the powder bed fusion technique. (B) A fully dense zirconia toughened alumina dental restoration with acceptable mechanical properties [87]. The dental restoration highlights a major challenge of PBF, poor surface finish.

strength significantly decreased as particle size was reduced from five to two μm , resulting in unstable parts. For particle sizes below five μm , powder should be agglomerated prior to coating with polymer.

Nelson et al. [86,87] modeled thermal diffusion within the powder bed for polymer coated ceramic materials. Polymer coating thickness showed the most significant effect on thermal properties; thermal calculations provide data to optimize scan speed, laser power, and raster width. The model was used to predict the flexural strength for green test bars produced using different processing parameters and showed good agreement with experimental 4-point bend testing results. The flexural strength of green test bars was found to increase linearly with energy density up to an elbow point at 1.2 cal/cm^2 , after which the rate of increase in strength reduces by 80%. This phenomenon is due to polymer degradation from excessive heating. This finding is important for any AM process that uses a laser for selective energy application to both liquid and powder beds. In order to address excessive heating, a thermal efficiency term, input energy density (IED), is introduced

$$\text{IED} = \text{energy density} * f \left(\frac{2\omega}{L} \right). \quad (2)$$

This term takes into account the energy density that material receives and the frequency of laser spot passes, where overlap will heat each location several times at different energy densities. This is important because heat is rapidly lost during a scanning cycle as the laser moves away from a specific point and then returns to pass over an adjacent area. Therefore, large parts will have a heating process with a lower thermal efficiency because each location has more time to cool during longer scan vectors.

In 1999, Gureev et al. [88] fabricated piezoelectric elements in the first reported direct PBF study. A stoichiometric mixture of TiO_2 , ZrO_2 , and PbO powders was sintered using a Nd:YAG laser with a spot size of $50 \mu\text{m}$. Laser powers between 11 and 14.5 W and scan speeds from 15 to 30 mm/s produced cohesive parts containing approximately 80 vol% porosity. Fabricated parts were annealed at $1240 \text{ }^\circ\text{C}$ for 3 h to enable PZT phase formation and reduce residual stresses. Annealing reduced porosity to approximately 75 vol%. Annealed parts showed piezoelectric properties but could only withstand a maximum electric field of 0.95 kV/mm ; above this threshold breakdown occurred due to porosity.

4.3. Recent developments

Thermoset binders were studied for used in ceramic PBF by Evans et al. [89] in 2004. Thermoset polymers cannot be remelted like thermoplastics, but instead leave a high volume-fraction of carbon when subjected to temperatures above their volatilization point. Phenolic resin was used to bond SiC powders due to its high carbon yield of 40–70 wt.%. Unlike the thermoplastic binders used in previous studies, phenolic resin maintains green body strength after pyrolysis; phenolic resin transforms into carbon ash with yields of 40–70 wt.% during pyrolysis. During sintering, the phenolic ash functions as a sintering aid and can even be used as a preceramic polymer when paired with metal infiltration.

In order to achieve high density and mechanical properties, Shahzad et al. [90] processed green alumina parts fabricated by PBF with pressure infiltration (PI) and warm isostatic pressing (WIP) before sintering at $1600 \text{ }^\circ\text{C}$. Alumina parts that were not processed with PI or WIP reached relative densities of 39% when sintered. Relative density was increased to 64% using PI (alumina-ethanol solution at 13 MPa) and 89% using WIP (64 MPa and $135 \text{ }^\circ\text{C}$). Interestingly, using PI and WIP together resulted in a lower relative sintered density of 88%. However, by infiltrating porosity before WIP, shrinkage is significantly reduced, which limits the potential for warping or cracking of complex geometries. An average flexural strength of $148 \pm 22 \text{ MPa}$ was achieved for these crack-free complex alumina parts. Similar work by Liu et al. [91] achieved complex alumina parts with relative densities of 92% by cold isostatic pressing printed green bodies and sintering at $1600 \text{ }^\circ\text{C}$.

In 2006, Gahler and Heinrich [79] demonstrated direct fabrication of alumina-silica ceramics with relative densities up to 92%. To achieve this density, a doctor blade was used to spread $100 \mu\text{m}$ layers of ceramic slurry, consisting of 50 wt.% silica, 16 wt.% alumina, and 34% water, which were selectively melted using a continuous-wave CO_2 laser. The alumina-silica system enabled crack-free specimens with narrow composition and laser parameter ranges. In a different direct PBF study, a low relative density of 56% was achieved for yttria stabilized zirconia parts due to the use of a lower power laser that caused partial melting, which resulted in net shaped parts of the same density as the powder bed [92]. An advantage of partial melting is the significantly lower thermal stresses, which enables the fabrication of larger parts, and the large volume-fraction of open porosity could be infiltrated to improve relative density.

Two decades after the first ceramic PBF studies, Hagedorn et al. [80] successfully demonstrated direct fabrication of fully dense oxide ceramic components with mechanical properties comparable to oxide ceramics produced through traditional routes. In order to reduce thermal stresses that cause cracking and part failure, a CO_2 laser was used to heat the entire $30 \times 40 \text{ mm}^2$ build area to above $1700 \text{ }^\circ\text{C}$. Complete melting of the ceramic powder was accomplished using a continuous-wave Nd:YAG laser. The rapid melting and cooling produced a fine-grained microstructure, resulting in a flexural strength of more than 500 MPa for $\text{ZrO}_2\text{-Al}_2\text{O}_3$ parts of 2.5 mm in height [81]. However, parts of height 10 mm had severe cracking due to thermal gradients between top and bottom layers. A three-unit dental restoration was fabricated using this technique and loaded to 1000 N without failure [93]. The dental restoration, Fig. 4B, highlights a major challenge of PBF, poor surface finish. Furthermore, heating the whole powder bed above the feedstock material's sintering temperature is expensive and difficult to scale.

5. Binder jetting for advanced ceramics

5.1. Foundations

Binder jetting, known under the trademarked name 3D Printing (3DP), was the very first AM process used for

producing ceramic parts. In fact, this was the only process created specifically for processing ceramic powders and then later adapted to metallic and polymeric materials [47]. To create a three-dimensional part, liquid binder is applied to selectively bind powder in a thin layer, loose powder is spread over the top, and the binding process is repeated. The binder jetting process is illustrated in Fig. 5A. Complex geometries with overhangs, which are supported by unbound powder, can be fabricated from any powdered ceramic material of appropriate particle size; powder smaller than 50 μm will agglomerate and inhibit flow [94]. Resolution is limited by powder size or binder droplet size, depending on which is larger. The excellent dimensional accuracy of the binder jetting technique is enabled by using nozzle orifices less than 50 μm . Binder rheology and nozzle geometry play important roles in controlling the size of droplets [95]. Binder can be applied through either drop-on-demand or continuous-jet techniques. Continuous-jet printers use a pressurized ink reservoir and a piezoelectric element to break the ink jet into droplets. Droplets are charged as they exit the nozzle and pass between electrodes, which allows them to be steered either back into the reservoir or onto the build platform by a strong electric field. For this reason, inks must be conductive for the continuous-jet process. Drop-on-demand printers use a piezoelectric actuator to produce a pressure pulse in the nozzle that

ejects droplets of ink and does not require conductive inks. The continuous-jet process produces droplets at a much faster rate (64 kHz), which enables a higher build rate compared with drop-on-demand systems.

5.2. Evolution

In 1990, Sachs et al. [33] performed the first additive manufacturing study using a non-polymeric material. Binder jetting was initially developed to print ceramic molds for casting metal parts with the goal to reduce the cost and lead-time of producing complex metal parts. In a traditional metal casting process, molds cost between \$5 k–50 k and can take several months to manufacture. While traditional molds enable high-volume production, binder jetting could provide significant benefit for unique, one-off parts. Build rate is determined by three main steps. First, powder spreading will take 0.1–1 s for dry powder and 1–10 s for wet powder. Second, printing a 0.5×0.5 m layer would take approximately 0.025 s for a continuous jet process and 5 s for a drop-on-demand process, if the head is designed with a line of jets so as to print in a single pass. Third, the binder must set, which is estimated between 0.1 and 1 s for solvent-based binders.

The physics of the ballistic impact of binder droplets into the powder bed has implications in x-y resolution, surface finish, mechanical properties, and even resolution in the build

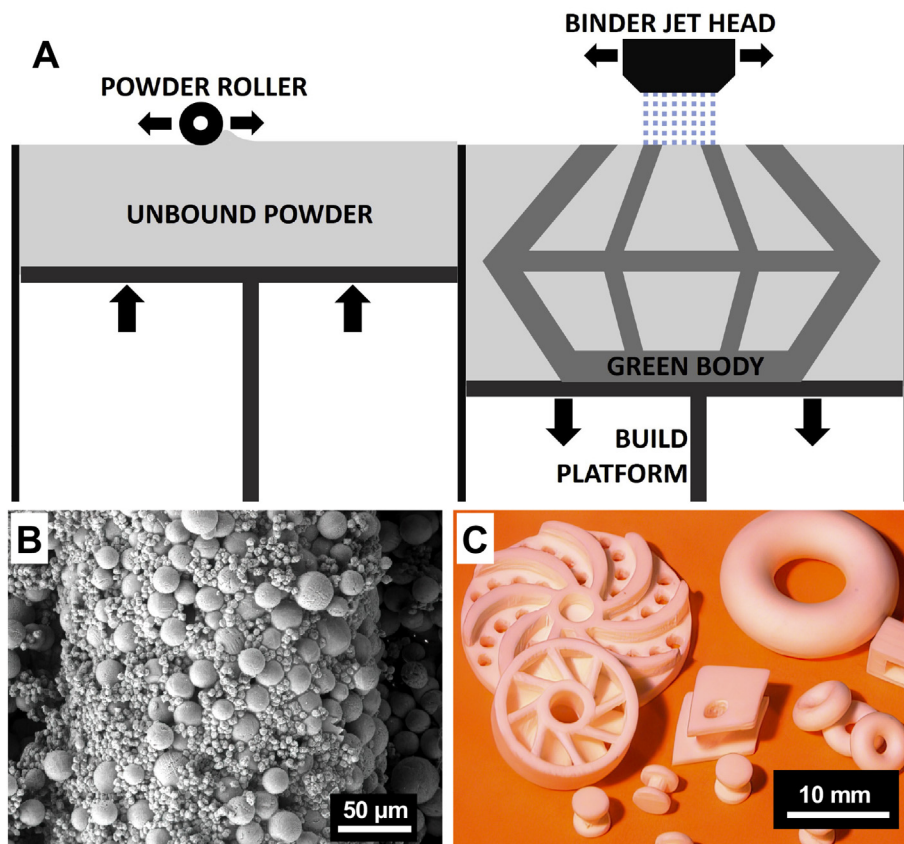


Fig. 5 – (A) Diagram illustrating the binder jetting technique, where a three-dimensional object is produced by selectively depositing binder droplets into a powder bed layer-by-layer as the build platform lowers and fresh powder is spread to create a loosely bound green body. (B) A bimodal particle size distribution enables better surface finish, and small particles tend to migrate to the surface [93]. (C) Several complex alumina parts with good surface finish and edge definition [93].

direction due to powder compaction. Droplet overlap and interaction provide the green strength necessary to maintain form after removing loose powder. Vertical dimensional error is caused predominantly by displacement from compaction of the powder bed due to the weight of subsequent layers. Increasing the packing density of the powder bed reduces this error. For a powder bed of packing density 54 vol% comprised of 30 μm alumina powder, vertical accuracy errors of approximately 50 μm were measured for middle layers [96]. Middle layers in a powder bed will always show the highest compaction displacement as sufficient weight from upper layers and sufficient room for displacement both exist. Powder scattering occurs due to the kinetic energy of the binder droplets, which reduces dimensional accuracy and surface finish. Powder scattering is significantly reduced for powder beds that are misted with water to loosely fix powder in place [97]. These alumina cores bound with silica are used to cast metal parts, such as turbine blades.

Yoo et al. [98] used binder jetting to produce ZTA parts with functionally graded yttria doping, with the goal of tailoring transformation toughening mechanisms. The binder jetting system utilized a multiple nozzle print head where either binder, binder-yttria ink, or a ratio of the two were jetted into the powder bed. By carefully controlling the yttria dopant composition, the ZTA phase was tailored locally between monoclinic and tetragonal. Multilayer composites with tailored internal stresses and transformation toughening were formed and pressureless sintered to 99% theoretical density. Post-processed parts showed an increase in flexural strength of 441 MPa, which indicates that compressive stresses were successfully developed at specimen surfaces.

5.3. Recent developments

Sachs et al. [99] demonstrated the use of ceramic powder with a bimodal size distribution to reduce surface roughness in 2003. Fine powders of particle size less than two μm improve surface finish and sinterability but cannot be spread dry due to Van der Waals forces. Fine powder must be spread wet in slurry form, which significantly slows the process and increases its complexity. On the other hand, coarse powders can be spread dry, but cause rough surface finish and poor densification during sintering. In this study, a bimodal size distribution of spherical alumina powder was spread dry and compared with results from a unimodal alumina powder. Coarse powder used measured 20 and 30 μm and fine powder used measured 2.5 and 5 μm . Coarse powders were mixed with 10–25 vol% fine powder and spread across the bed. Surface roughness is significantly reduced using the bimodal distribution as seen in Fig. 5B. Interestingly, fine particles tend to migrate to the surface as the binder droplet selectively binds material, which explains the reduction in surface roughness. In addition to improving surface finish, a wider particle size distribution can increase green body density. Several complex alumina parts (Fig. 5C) were fabricated with good quality and edge definition. Gonzalez et al. [100] produced alumina parts with relative density of 96.51% and compressive strength of 146.6 MPa, by using a bimodal particle

size distribution. Kunchala et al. [101] added nanoparticle densifiers to the liquid binder to improve green body density. Alumina green bodies with nanometer-sized alumina particles were produced with a relative density of 65.7%, compared to green bodies without nanoparticle additions that had a relative density of 35.7%. Although these parts were not sintered, the significant increase in green body density indicates sintered density and mechanical properties would greatly improve via nanoparticle additions.

Recently, II–VI MCubed demonstrated binder jetting of SiC preforms that were subsequently reaction bonded (RB) with Si [102]. SiC preforms with dimensions of $4 \times 4 \times 0.25$ inches were fabricated using binder jetting. Preforms were printed using SiC feedstock powder with monomodal and bimodal particle size distributions. The printed preforms were then infiltrated with molten Si at a temperature above 1410 °C in an inert atmosphere to form SiC–Si composites. The density, elastic modulus, flexural strength, and fracture toughness of all printed and RB specimens increased with volume fraction SiC. Specimens fabricated using bimodal feedstock powders had higher density, elastic modulus, flexural strength, and fracture toughness at all tested volume fraction SiC. Compared to traditionally formed and RB SiC, specimens formed via binder jetting and then RB had comparable density, elastic modulus, and flexural strength, but lower fracture toughness.

6. Material jetting for advanced ceramics

6.1. Foundations

Material jetting, originally named ballistic particle manufacturing, uses ink-jet printers with nozzle diameters in the range of 20–75 μm to print low viscosity ceramic particle suspensions, termed ‘inks’ [103]. Material jetting is depicted in Fig. 6A. There are two main methods of material jetting, drop-on-demand and continuous-ink-jet. If a multi-nozzle printing head has separate reservoirs with different inks, composition can be varied to create functionally graded parts. Material jetting of ceramic materials is difficult because ink formulation must follow conflicting requirements, such as the ink needing to be low enough viscosity to avoid nozzle clogging while also containing enough ceramic content that the green body can be sintered to full density. Material jetting enables the use of ceramic materials of particle size less than 100 nm that are well dispersed as inks. Using these ultra-fine powders promotes sintering to enable full-density parts after post-processing.

6.2. Evolution

In 1995, Blazdell et al. [104] produced three-dimensional yttria stabilized zirconia parts using the material jetting process. A 70 μm nozzle array was used with the capability to dispense 50,000 droplets per second. Printed traces and thin wafers were pyrolyzed and sintered, and were free from printing defects, cracks, and shape distortion effects. In 1997, Teng

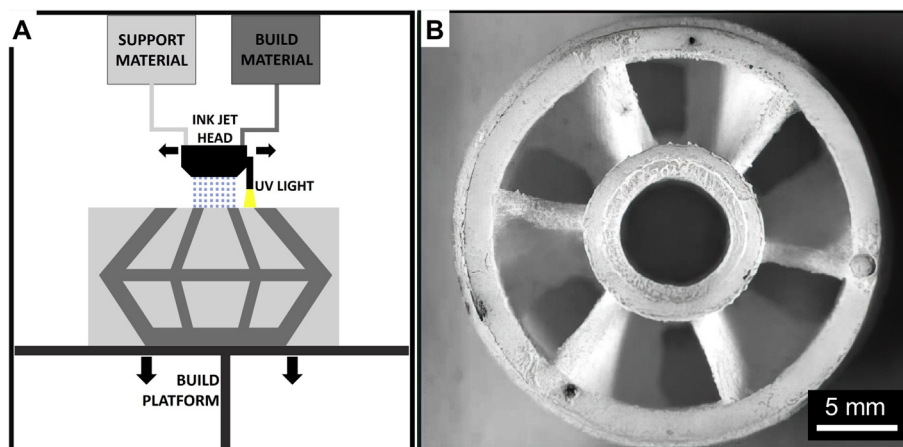


Fig. 6 – (A) Diagram illustrating the material jetting technique. (B) Alumina impeller produced by material jetting of a highly-loaded ink [101].

et al. [105] used continuous-ink-jet printing to create ceramic green bodies. Ceramic inks used for jet printing ceramic components must be well dispersed and dilute to have an acceptably low viscosity. However, it is important to load the maximum possible volume fraction of ceramic material into inks to produce high density green bodies that can be sintered into dense ceramic parts. In addition, inks must be conductive to enable the steering and detection of droplets during the jetting process. For these reasons, the development of optimal ceramic inks for jet printing is vital to the success of the material jetting technique.

Inks should have a conductivity of greater than 0.1 S/m, viscosity between 1 and 10 mPas, surface tension between 25 and 70 mN/m, and particle size less than 1 μm . Teng [105] found that an ideal ink composition contained 2.4 vol.% grade HSY3 submicron ZrO_2 powder, 1.43 wt.% ATSURF dispersant, and remainder ethanol as the solvent. To increase the conductivity of the ink, ethanol was modified with 2 wt.% ammonium nitrate. The optimal ink formulation had a conductivity of 0.298 S/m and viscosity of 1.64 mPas. The jetting nozzle had a diameter of 65 μm . Ceramic green bodies with acceptable dimensional resolution were successfully fabricated using this ink.

Two years later, Song et al. [103] developed ZrO_2 components of height 2.5 mm (1700 layers) using a continuous-ink-jet printer with nozzle diameter 60 μm . The development of an optimal ink formulation was focused on and resulted in an optimally functioning ink with 4.4 vol.% ZrO_2 . The ZrO_2 powder (grade HSY3) was stabilized with 5.4 wt.% yttria of particle size 100 nm. Printed parts were pyrolyzed and sintered at 400 and 1450 $^\circ\text{C}$, respectively. Viscosity must be below 100 mPas to avoid satellite formation during droplet ejection; satellites are small drops that break off the main droplet. Ink formulations dispersed solely using ultrasonic agitation were found to clog nozzles and cause irregular droplet ejection; powder agglomerates were not eliminated. In order to fully breakdown agglomerates, a twin-roll mill was used for high-shear mixing of subsequent formulations and resulted in consistent droplet formation and avoided nozzle clogging. Compared with passive drying, surface quality and dimensional accuracy was

found to be improved by active drying via hot air flow after each layer is deposited. Although bulk shapes were achieved, walls were not vertical and surfaces are dimpled and curved.

6.3. Recent developments

In order to solve issues related to printing low ceramic content inks, such as poor surface finish and dimensional accuracy, in 2001 Seerden et al. [106] formulated wax-based ceramic inks with up to 40 vol.% ceramic powder that were successfully ejected from an ink-jet head. Optimal formulations contained 20–40 vol.% Al_2O_3 powder (400 nm diameter), 0.65–1.2 wt.% surfactant Hypermer LP1, 0.33–1.2 wt.% stearylamine, and remainder paraffin wax. Optimal printing conditions were 100–110 $^\circ\text{C}$ and 10–13 kHz droplet frequency. In order to successfully print the 40 vol.% formulation, pressure was applied to the ink reservoir to aid the piezoelectric actuator driven pressure pulses. Ceramic green bodies were developed using the drop-on-demand method with feature sizes of less than 100 μm using an ink with 30 vol.% ceramic content. Fabricated green bodies showed good shape retention and dimensional accuracy, with vertical walls and sharp corners well defined.

Reis et al. [107] tested ZrO_2 and PZT using paraffin wax based inks with the drop-on-demand method. Sintered bodies retain features such as corners and vertical walls, and no warping, cracking or delamination is observed as illustrated in Fig. 6B. The use of thermal energy to lower the viscosity of wax-based ceramic inks shows great promise for increasing the maximum ceramic content of material jetting processes, which enables to development of dense, structural ceramic components. Driving pressure must be carefully controlled to eject uniform droplets of the high viscosity wax-based ceramic inks; relevant parameters include electric signal voltage amplitude, frequency, pulse duration, and waveform. Acoustic pressure wave superposition of two or more consecutive waves are necessary to provide the necessary energy to eject droplets of high viscosity ink [108]. A relationship is outlined between ejected drop volume and velocity and a dimensionless quantity Z ,

$$Z = \frac{(d\rho\gamma)^{0.5}}{\eta} = Oh^{-1}, \quad (3)$$

where d is nozzle diameter, ρ is ink density, γ is ink surface tension, η is ink viscosity, and Oh^{-1} is the inverse of the Ohnesorge number. Fromm [95] used this relationship to predict that droplet formation in DOD systems is only possible for $Z > 2$ and that droplet volume increases with increasing Z .

Dense PZT components with good shape retention were fabricated using a wax-based ceramic ink with a PZT content of 35 vol.% [109]. The optimal ink formulation contained 35 vol.% PZT (particle sizes less than 500 nm), 1% polyester, 0.5% stearylamine, and remainder paraffin wax. To further reduce the viscosity, solid paraffin wax was replaced with a 60/40 paraffin oil/wax mixture. A porosity of less than 1% was achieved for sintered components.

7. Sheet lamination for advanced ceramics

7.1. Foundations

Sheet lamination, commonly called layered object manufacturing (LOM), involves the cutting and layering of prefabricated ceramic tapes, often made via tape casting, into three-dimensional parts. A rectangular block is produced containing the desired object surrounded by 'tiled' support material. The 'tiled' regions are produced by cutting the negative space around the desired shape into a grid. Blocks of green material are then sintered and de-cubed, wherein support cube grids are mechanically removed to extract the final geometry. Sheet lamination is depicted in Fig. 7A. The process of tape casting thin ceramic sheets was patented in the 1940s to enable the mass production of capacitor dielectrics [110,111]. The idea of layering ceramic tapes, cut to specific

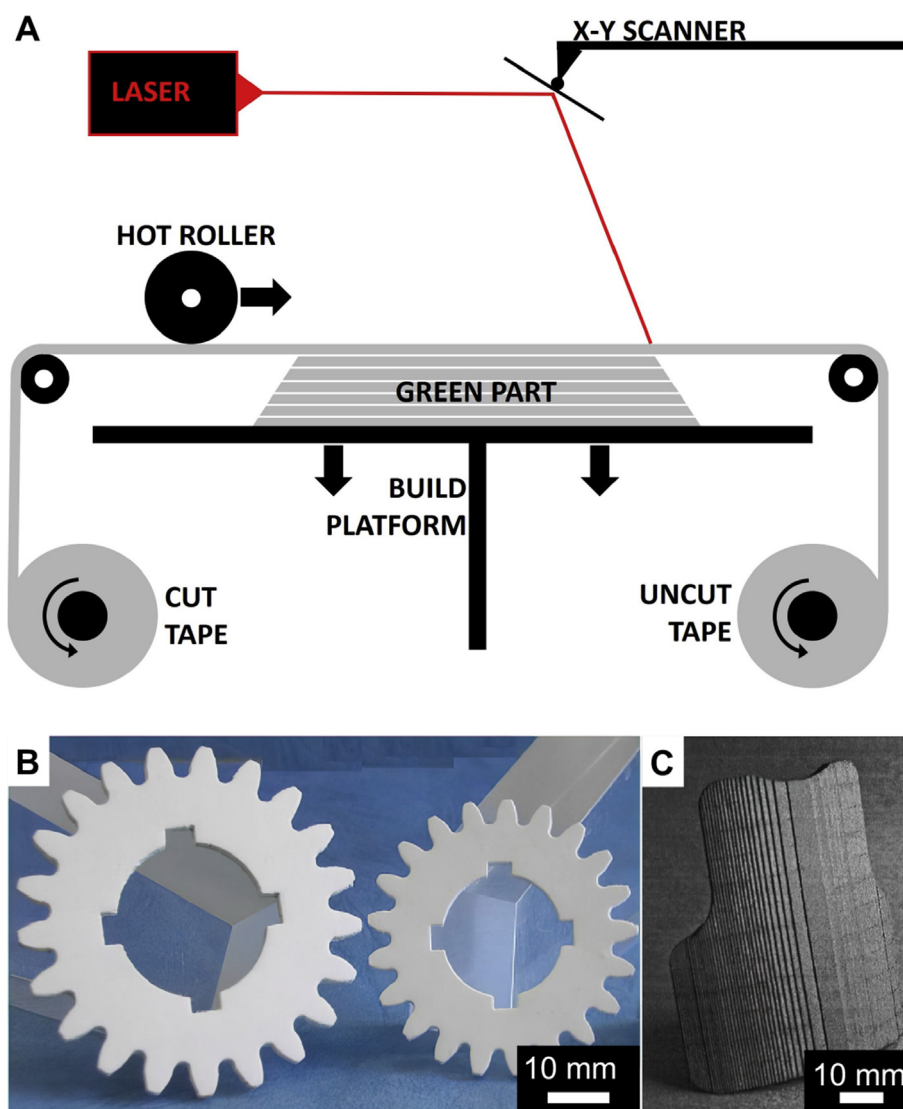


Fig. 7 – (A) Diagram illustrating the sheet lamination technique. (B) Glass-ceramic gears in green (left) and sintered (right) state demonstrating successful densification without warping or cracking [114]. (C) Complex curved SiC component produced by sheet lamination of bimodal SiC tapes [109].

geometries, was patented in the 1960s [112]. Interestingly, the commercial application of layering ceramic tapes for the production of three-dimensional parts lagged for nearly 30 years, when sheet lamination was patented in 1988 [44]. The reason for this lag in application is primarily due to the limited control of laser scanning equipment and software that could convert a 3D model into slices and motion planner to raster the laser in an efficient automated process to build parts. Sheet lamination processes face challenges related to the quality of interfaces, where defects such as delamination, porosity, and thermal-stress induced cracking cause failure of components.

7.2. Evolution

In 1991, Feygin et al. [45] and Helisys, Inc. first demonstrated the use of sheet lamination for producing three-dimensional parts; many materials were successfully demonstrated including ceramics, paper, plastics, composites, and even metals. In 1994, Griffin et al. [113] fabricated advanced structural ceramic components with complex geometries using LOM. In order to verify the mechanical performance of printed parts, rectangular bars of alumina were prepared by LOM and traditional dry-pressing. Alumina sheets for LOM were produced by casting a slurry with a doctor blade into 15 μm thick green tapes. Green tape is loaded onto the supply roll and fed over the build platform. A laser is used to cut a grid outlining the desired shape, which can be easily removed in post-processing steps. Heat and pressure are applied to each layer to aid layer lamination. Both pressed and LOM'ed parts were pyrolyzed at 600 °C to remove organic material and then sintered at 1550 °C for 2 h. Specimens from both processes sintered to full density with less than 1% porosity. Flexural strength, hardness, and fracture toughness values for the LOM'ed bars were all within one-standard deviation of those for the traditionally processed bars. Expanding on their previous work, Griffin et al. [114] fabricated complex ceramic $\text{ZrO}_2\text{-Al}_2\text{O}_3$ composites. Two different thicknesses, 58 and 116 μm , of tapes were produced with compositions of Ce– ZrO_2 and Ce– $\text{ZrO}_2/\text{Al}_2\text{O}_3$. Composite parts were developed by alternating layers of the two compositions. Green bodies were post-processed by pyrolysis and then sintering at 1600 °C for 6 h. Final parts contained less than 1% porosity and no delamination of macroscopic defects were observed. Final layer thicknesses in densified parts were approximately 85 and 44 μm for starting tapes of thicknesses 116 and 58 μm . Comparing monolithic parts to composite parts, the flexural strength increased 20% by alternating composition layer-by-layer. Complex geometries with curved and vertical surfaces were successfully produced with composite structures. Hardness varied locally with composition.

Three ceramic systems were studied by Klosterman et al. [115] in 1996: (1) Coarse SiC powder of size 30 μm that enables post-process infiltration; (2) Bimodal SiC with particle sizes 2 and 30 μm ; and (3) AlN powder with particle size 2 μm . Ceramic feedstock material was prepared using a standard tape casting process. A slurry consisting of 60 vol.% ceramic powder, binder, plasticizer, and solvent was cast into tapes of thicknesses 150–175 and 300–325 μm . Ceramic tapes were manually loaded into the sheet lamination system. In order to

prevent the oxidation of these carbide materials during the sheet lamination process, a blower supplies an inert gas at the focal point of the laser to shield the cutting process. In order to increase the green strength of LOM'ed parts, a particle binder burnout cycle was run that volatilized the plasticizer but left the binder. Subsequent silicon infiltration and reaction bonding resulted in near net-shape parts with little dimensional change, shown in Fig. 7C. However, poor layer bonding led to delamination and a relatively low flexural strength of 160 MPa. In comparison, SiC components produced via binder jetting and reaction bonding have flexural strengths of approximately 280 MPa [102].

Himmer et al. [116] demonstrated an automated tape casting process connected to a sheet lamination system in 1997, eliminating the need to manually place feedstock material. Plastic was rolled over the top of ceramic slurry into 0.25 mm thickness sheets, which avoided the need to let the slurry dry into a solid tape. In this fashion, a continuous layer of slurry and plastic was fed into the sheet lamination system, where the plastic was then separated from the layer of slurry. Complete separation is important, because any slurry that sticks to the plastic will leave voids in the laminated part. Parts with complex geometries were built to up to 20 layers successfully. After pyrolysis and sintering parts contained 10–15% porosity, which led to low strength and delamination. Macroscopic voids were observed due to incomplete plastic-slurry separation prior to sheet lamination.

Klosterman et al. [117] published a follow-up study in 1998 focused on improving the interfacial bonding of laminated sheets. SiC tapes were produced using a doctor-blade and slurry containing bimodal SiC powder (2–3 and 60 μm particle sizes), graphite powder, and binder system. The lamination roller was set to 180 °C, above the binder melting point, to achieve sufficient interlayer bonding. Pyrolysis at 600 °C and reaction bonding with silicon at 1600 °C produced near-net-shaped parts. A low flexural strength of 80 MPa (compared to the expected 300–400 MPa) was measured. Large voids were observed at layer interfaces. Strength was increased to 155 MPa by increasing the graphite powder content from 5 vol.% to 20 vol.%. In order to further improve strength, the layer bonding needs to be improved. To improve bonding, a solvent was misted on the tape prior to lamination and the temperature and pressure of the lamination roller were increased. Using these methods, interlayer bonding was improved to the point that parts could not be de-cubed. It was found that a secondary cutting operation around the profile of each layer, after creating the support grid, enabled successful de-cubing even at higher lamination pressures and temperatures. This operation left a thin layer of powder at the interface between cubed support regions and the desired part, which facilitated the removal of the cubed material. Through the use of the secondary cutting operation and better lamination parameters, defect free layer interfaces were demonstrated.

7.3. Recent developments

Rodrigues et al. [118] fabricated silicon nitride parts using the sheet lamination process in 2000. They found a direct correlation between the feedstock quality, i.e. homogenous ceramic tapes with uniform thickness, and the mechanical

properties of final parts. In addition, lamination roller pressure and temperature were carefully optimized to yield sufficient interlayer bonding. LOM'ed parts were pyrolyzed at 500 °C and sintered at 1750 °C, resulting in less than 3% residual porosity. The flexural strength and fracture toughness of silicon nitride parts produced with sheet lamination matched that of silicon nitride parts made using traditional methods. Fracture surfaces reveal complete layer bonding and no interlayer defects are observed. Travitzky et al. [119] tape casted preceramic polymers filled with SiC of varying particle sizes, and fabricated functionally graded ceramics using the sheet lamination technique. SiC structures with graded particle size showed 25% higher flexural strength over those produced with uniform particle size. Gomes et al. [120] increased the strength of glassy ceramic components by rotating feedstock tape by 90° for each layer of the sheet lamination process. Complex $\text{Li}_2\text{O}-\text{ZrO}_2-\text{SiO}_2-\text{Al}_2\text{O}_3$ green parts were sintered at just 700 °C and achieved near full density, shown in Fig. 7B.

That same year, Park et al. [121] characterized the LOM process to determine important sources of dimensional error. Error was found to be largest in the build direction due to moisture absorption and subsequent tape swelling. Low relative humidity during the forming process was found to be important. Two years later, Karunakaran et al. [122] proposed an efficient method for separating the desired object from the surrounding block of material. A major drawback of the sheet lamination process is the significant time of cutting the support grid and then de-cubing the fabricated part. Their method is analogous to extracting a casting from a mold, where the mold primarily consists of two halves and can contain plugs to create internal cavities. Instead of making many cuts to form a grid, the negative space of each layer is cut into two halves. The cuts are coordinated across layers to create a consistent seam that enables the separation of the support material in two pieces, compared with many cubes in the traditional sheet lamination process.

Weisensel et al. [123] demonstrated the fabrication of biomorphic ceramic composites via the sheet lamination technique, with the goal of mimicking natural cellular materials. A cellulose based paper was used with a phenolic resin adhesive. After laminating several layers and creating a three-

dimensional part, the paper and phenolic resin were pyrolyzed to leave a layered carbon structure with porosity templated from the natural cellulose structure. Through reaction melt infiltration with silicon, the carbon structure was converted to a Si–SiC composite with 16 vol.% residual carbon and negligible porosity. A flexural strength of 130 MPa was measured by four-point bend testing. To further increase the mechanical properties of these biomorphic composite structures, the melt infiltration process should be optimized to fully react with the carbon template.

8. Material extrusion for advanced ceramics

8.1. Foundations

The material extrusion process, commonly known as Robocasting, involves the extrusion of a high ceramic content slurry through a nozzle in a specific pattern layer-by-layer to produce a three-dimensional part [124]. This line of deposited material is known as a trace. Material extrusion is demonstrated in Fig. 8A. The material can be extruded continuously or in droplets, and self-supports via gelation, cooling, UV-curing, or other rheological effects [125]. Yield-pseudoplastic rheology enables the ink to retain structural integrity up to its yield stress, followed by shear-thinning behavior [34,126]. This behavior is critical for ink to both flow through a small nozzle (high-shear environment) and retain its shape post-extrusion (low-shear environment). Advantages of the material extrusion technique include low-cost machinery, versatile feedstock, and high green density. Challenges include achieving small feature size, low precision, and poor surface finish.

8.2. Evolution

In 1995, Danforth's group [127] developed the fused deposition of ceramics (FDC) method in the Center for Ceramic Research at Rutgers University. The feedstock material used in this process is thermopolymer filament loaded with ceramic powder. FDC is analogous to fused deposition modeling, developed by Stratasys, where thermopolymer filament is

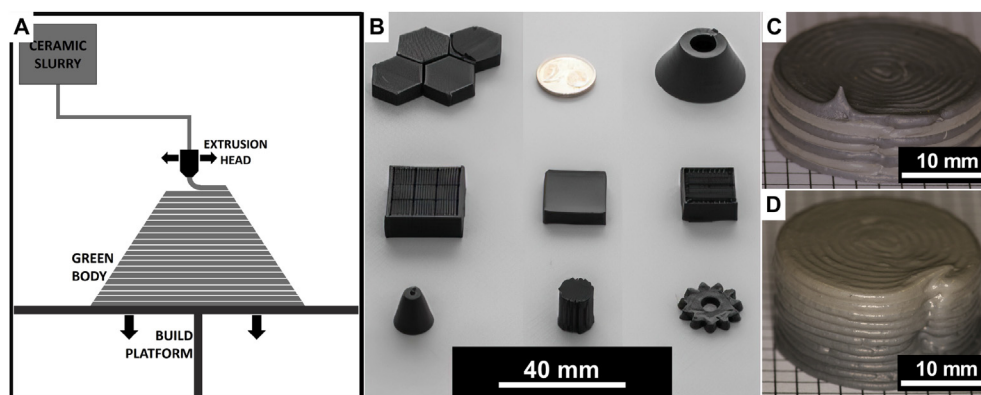


Fig. 8 – (A) Diagram illustrating the material extrusion technique. (B) Complex boron carbide components were processed using spark plasma sintering and cold isostatic pressing to achieve less than 5% residual porosity [133]. (C, D) Discrete and continuous SiC–B₄C parts printed using a material extrusion system with in-line mixing capabilities [25].

melted and extruded to build plastic parts. Thermoplastic filament loaded with 55 vol.% Si_3N_4 was printed and sintered to greater than 98% relative density and average flexural strength of 824 MPa [128]. Printing defects are a major concern for material extrusion processes, because inconsistent tool-path generation can cause large voids between traces of printed material [129]. During the creation of simple testing geometries, toolpath files can be manually optimized to reduce defects. However, manual modification is not possible for more complicated geometries.

Kupp et al. [130] used a different approach termed multi-phase jet solidification (MJS), where a thermoplastic-ceramic mixture is directly fed through a heated nozzle using a piston. Time-consuming filament production is avoided in this technique. The feedstock material contains 50–70 vol.% ceramic material. Fabrication of SiC parts with complex geometry was successfully demonstrated.

A year later, Cesarano and Grieco [131] conducted a high-impact material extrusion study using ceramic materials at the Sandia National Laboratory. This study termed the common name of Robocasting for the material extrusion of ceramic slurries. His motivation was to increase the green density of ceramic AM parts to improve post-processing behavior, namely debinding and sintering processes. Slurries of 50–65 vol.% ceramic and less than 1 vol.% organic were developed and successfully printed. In contrast with ceramic parts made in binder jetting and vat photopolymerization processes, these parts could be post-processed in less than 24 h versus several days due to the much lower organic content. In addition, the high ceramic content enabled sintering to higher relative density and less shrinkage, resulting in improved final properties. Producing ceramic slurries of such high ceramic content faced several technical challenges including difficult rheological control and drying kinetics. Previous work by Cesarano and Aksay [132] discussed the development of aqueous alumina suspensions and provided a basis for the slurries printed at Sandia National Laboratory. Well-mixed suspensions of alumina, Darvan-821 A, and water showed yield-pseudoplastic behavior for ceramic content below 60 vol.%, followed by dilatant behavior. Low viscosity and slow drying results in slumping, whereas high viscosity and fast drying enables good shape retention. Robocasting suspensions exhibit significant yield-pseudoplastic behavior during printing, but quickly change to dilatant behavior after extrusion and minimal drying to retain their specified geometry. Alumina geometries were made by Robocasting of yield-pseudoplastic ceramic slurries. Finite element analysis (FEA) simulations indicate fast drying results in good shape retention, voids form for medium drying rates, and low drying rates lead to significant slumping [133].

In 2000, Lewis et al. [19] conducted an in-depth rheological study of colloidal ceramic suspensions, with the goal of enabling Robocasting with smaller nozzles, improving shape retention, and producing defect-free parts. Technical challenges faced included isolating printing and rheological parameters. To perform this study, a mixing system was designed that allowed for on-the-fly binder content adjustment in the printed slurry. This methodology enables high-throughput discovery of the optimal ceramic content in extruded slurries for different powdered materials. The

viscosity of several notable slurry compositions was measured across a range of shear rates, with an emphasis on isolating the shear rate for each step in the printing process. Four printing process steps were identified as pumping, mixing, extrusion, and deposition. In addition, FEA simulations were used to verify shear-rate regime calculations. Through this work, alumina slurries were successfully printed from nozzle sizes 0.254–1.370 mm and showed good shape retention with no observable defects.

8.3. Recent developments

Jafari et al. [134] developed a multi-head FDC system, capable of printing up to four unique ceramic loaded thermoplastic filaments. Two filaments, one loaded with PZT-5H and one loaded with PZT-8, were used to produce multilayer parts with alternating layers of the two piezoelectric materials. The dielectric constant of the parts was tunable based on the ratio of PZT-5H to PZT-8, with applications for improving the performance of transmitting devices. Smay et al. [135] conducted a comprehensive multi-material study using two types of machine set-ups, a multi-head arrangement where each tool head deposits a different material and a single head arrangement where active mixing inside of the tool head enables the tailoring of composition to any ratio of the feedstock materials. The motivation was to create cermet materials and ternary composition gradients. Technical challenges faced include difficulty in controlling the rheology of multiple input materials where differences in viscosity or compressibility will cause poor printability and variation in surface chemistry between metallic and ceramic powders. Printing ternary mixtures of barium titanate, strontium titanate, and barium zirconate, requires the rheology of each material to be matched across a range of shear rates that the slurries experience during processing. Both ternary mixtures and cermets were demonstrated and showed good final properties after post-processing. Pelz et al. [28] fabricated functionally-graded carbide parts using a print head with an extrusion screw to mix two feedstock materials in-line. Discrete and continuous composition variation were demonstrated as shown in Fig. 8C,D. Full density was achieved, and hardness values match traditionally processed carbide materials. A part with alternating SiC and B_4C layers was printed but cracked due to residual stress arising from coefficient of thermal expansion mismatch.

Iyer et al. [136] produced strong, dense Si_3N_4 components using the FDC technique. Filament contained 55 vol.% Si_3N_4 (average particle size of 0.5 μm). Printing parameters include a nozzle width of 250 μm , layer height of 254 μm , and x-y or z testing bar orientations. After sintering, the full density Si_3N_4 bars printed in the x-y and z orientations had flexural strengths of 908 and 888 MPa, respectively. The near-isotropic strength of these parts is very promising and indicates printing defects are nonexistent and layer lines are fully eliminated during sintering. Rueschhoff et al. [137] used a low-cost (\$2 k) commercially available material extrusion printer to produce strong, dense alumina parts. Slurry compositions from 51 to 58 vol.% ceramic content were formulated with 5 vol.% binder content. The rheology of each suspension was characterized and it was found that a composition of 55 vol.% alumina, 4.2

vol.% Darvan 821 A, and 4.9 vol.% PVP produced the best print results. Post-processing included debinding at 700 °C and sintering at 1600 °C with no sintering additives or applied current or pressure resulted in parts with greater than 98% relative density. These parts showed flexural strengths comparable to those of traditionally processed alumina parts. In a second study, boron carbide suspensions were formulated using the same low-cost extrusion system [138]. A major motivation for this research is the fact that dense B₄C parts cannot be made using other AM techniques, such as vat photopolymerization (very high refractive index difference) or binder jetting (low density green bodies). The rheology of each suspension was characterized and it was found that a composition of 54 vol.% B₄C, 5 vol.% PEI (25 k g/mol), and 5 vol.% HCL enabled optimal printability. The binder PEI was tested at two different molecular weights, 25 k and 750 k g/mol, and it was found that the lower molecular weight results in a lower apparent viscosity. Good layer adhesion and shape retention were achieved, with limited shrinkage and warpage during post-processing. Parts were debound at 500 °C and sintered at 2000 °C with no sintering additives or applied pressure, resulting in parts of 82% relative density. This low relative density is due to the strong covalent bonding in carbide ceramics, which leads to very high melting temperatures. Eqtesadi et al. [139] demonstrated improved results for material extrusion of B₄C materials, producing complex geometries such as gears, cones, and hexagons (Fig. 8B). In order to create fully dense sintered specimens, green prints were first cold-isostatic pressed. This increased green density from 53% to 58% of theoretical. Green bodies were then densified via spark plasma sintered at 2100 °C to produce specimens with less than 5% porosity.

A unique characteristic of material extrusion processes is the pressure gradient in the nozzle, which enables the alignment of fibers and high aspect-ratio particles [140–144]. Bismuth titanate structures with oriented microstructures were fabricated by Allahverdi et al. [140] using the FDC technique to align BiT platelets. Using this technique, ceramic matrix composites were developed by Franchin et al. [141], which involved a SiC suspension loaded with 30 vol.% chopped carbon fiber. Fibers inside the SiC matrix reduce cracking that occurs due to post-processing. Fiber direction can be varied within a layer based on trace pathing. A maximum fiber loading of 30 vol.% was achieved due to rheological effects. Feilden et al. [142] used the nozzle pressure gradients, unique to material extrusion techniques, to align alumina platelets in epoxy-ceramic composites to create bioinspired structures. Bouligand structures, analogous to those in fish scales, with high ceramic content were produced. Upon loading and cracking, the structure guides crack propagation in a three-dimensional twisting motion that improves the toughness. Fabricated structures outperform the strength of nacre by a factor of two while maintaining a similar R-curve behavior (representative of toughening mechanisms that inhibit crack propagation). Kemp et al. [144] printed SiC fiber reinforced ZrB₂ components, which can function as structural ultra-high temperature ceramics. However, at 10 vol.% SiC fiber content, significant porosity developed, and mechanical performance was limited.

9. Directed energy deposition for advanced ceramics

9.1. Foundations

Directed energy deposition (DED), commonly known as laser cladding [145] or laser engineered net shaping (LENS) [145,146], uses a laser to melt powder or wire feedstock in layer-by-layer traces to build a three-dimensional part. This process is similar to welding, where a melt pool is formed by melting feed wire and is depicted in Fig. 9A. DED is the only ceramic AM process that is solely a single step process, which means parts formed do not require post-process densification. However, the use of DED for fabrication of bulk ceramic parts is limited due to thermal cracking, which results from the rapid heating and cooling in the melt-pool induced by the laser. This effect is similar to that previously described for single-step powder bed fusion. Further, poor surface finish and dimensional stability are occur due to freeform fabrication with complete melting. Interestingly, the authors did not

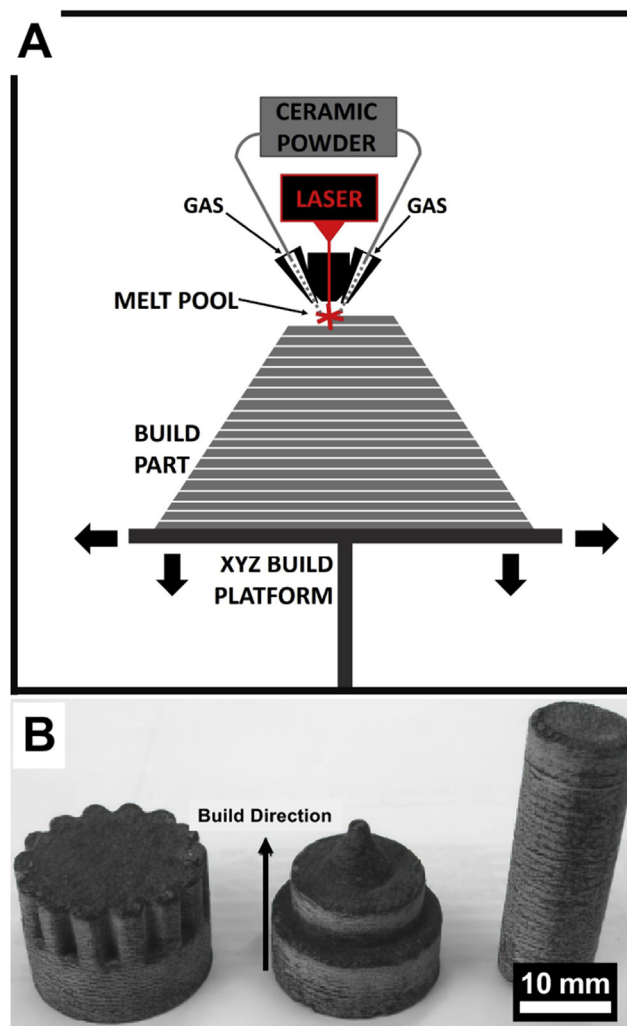


Fig. 9 – (A) Diagram illustrating the directed energy deposition technique. (B) Complex alumina components fabricated by DED, including a cylinder with a maximum dimension of 25 mm [139].

find a ceramic DED study that reported flexural strength, while fracture toughness was often reported.

9.2. Evolution

The first published account of a ceramic DED process studied the selective area laser deposition (SALD) method in 1993, which uses a laser to selectively heat a substrate and cause material deposition based on precursor gas, the feedstock material. Using tetramethylsilane as the precursor gas, Tompkins et al. [147] demonstrated small SiC deposits could be made selectively onto an alumina substrate. A second study of the SALD process by Jakubenas et al. [148] used TiCl_4 gas to selectively deposit titanium oxide. Deposit morphology is highly dependent on oxygen concentration in the precursor gas; low oxygen content leads to smooth deposits and high oxygen content results in dendritic depositions. However, in both studies the build heights were limited to a single layer because large thermal gradients caused cracking and irregular growth when printing a second layer. Fessler et al. [149] created a gradual, graded composition change using the directed energy deposition process and utilized a powder mixing system. Through gradual composition change, thermal gradients were reduced, and cohesive parts were successfully fabricated.

A similar method is the selective area laser deposition vapor infiltration (SALDVI) approach, where powder is fused together using a selective chemical vapor deposition process. Crocker et al. [150] demonstrated this technique using tetramethylsilane as the precursor gas to selectively infiltrate SiC into Mo, SiC, ZrO_2 , and WC powder beds. A laser is used to selectively deposit SiC into the powder bed, layer by layer, to create multi-layer parts. A rectangular part with four 250 μm thick layers was produced from tungsten carbide powder fused with the infiltrated silicon carbide. To obtain a sufficient infiltration depth, slow laser scan speeds must be used. However, at low scan speeds, SiC was not deposited evenly. Due to these competing factors, fabricated parts had poor surface finish and large voids.

9.3. Recent developments

In 2008, Balla et al. [145] first demonstrated the successful production of bulk alumina ceramics by the LENS technique. Fig. 9B shows several complex parts fabricated by DED, a maximum dimension of 25 mm was achieved. Fabricated alumina parts had relative densities near 96%, and through a short heat-treatment at 1600 °C relative density was increased to 98%. Heat-treated parts had average compressive strengths of 276 MPa. To create bulk parts that did not fail due to the large temperature gradients intrinsic to direct energy deposition processes, precise thermal management of the melt pool was performed. Niu et al. [146] again studied directed energy deposition of alumina, but with the addition of zirconia and yttria dopants to reduce processing defects and improve the microstructure. Fully dense parts of 50 mm in height were successfully fabricated. Fully dense parts with nanometer-sized eutectic microstructures were developed by the combined doping of alumina with zirconia and yttria [151]. A eutectic grain structure of spacing 100 nm was achieved,

resulting in high hardness (17.15 GPa) and fracture toughness (4.79 $\text{MPa}\cdot\text{m}^{1/2}$). Hu et al. [152] used the directed energy deposition process to create functionally graded ZTA parts. Zirconia contents were varied from 5 to 40 wt.%, which enabled the local tailoring of both different microstructures and phases locally. Through phase control of the heterogeneous structure, both toughness and hardness were improved. Adding 20 wt.% zirconia improved the hardness by 6.1%, but additional zirconia additions lowered hardness in comparison with monolithic alumina specimens. Fracture toughness increased consistently with increasing zirconia content with a maximum improvement of 38.2%, equal to 3.7 $\text{MPa}\cdot\text{m}^{1/2}$, at a dopant level of 41.5 wt.% zirconia. Hu et al. [153] used an ultrasonic vibration assisted directed energy technique to produce bulk ZTA parts. Cracks that developed in parts fabricated without vibration were not present in parts made using identical processing parameters but assisted by ultrasonic vibration. Cracking is reduced because ultrasonic vibration reduces thermal gradients and refines grain size. Grain size was refined from 16 to 8 μm by the application of vibration, which increases nucleation rate in the melt pool during DED processing. Hardness and compressive strength were both improved for parts fabricated by vibration assisted DED. In addition, ultrasonic vibration improves optical absorptivity, resulting in 9% energy savings compared to non-assisted DED techniques [154]. Yan et al. [155] produced nanometer-sized eutectic ZTA microstructures with spacing 60–70 nm. The fully dense parts had residual compressive stress at their surface due to DED processing, which resulted in a high fracture toughness of 7.67 $\text{MPa}\cdot\text{m}^{1/2}$.

10. Conclusions and future directions

10.1. Conclusions

Whereas metal and polymeric AM has experienced great success for both prototyping and industrial production, ceramic AM remains in the research and development phase due to the difficult processing conditions intrinsic to ceramic materials. Nevertheless, great progress has been accomplished for several ceramic AM techniques. Seminal papers for initial research efforts for each family of additive manufacturing processes were examined and their major findings, breakthroughs, and challenges were discussed. Progress in the 1990s centered around basic technique advancements, processing parameter optimization, and process modeling. This led to the production of dense, mechanically sound parts and expansion of the material selection. Recent efforts focus on novel structuring, multi-material capabilities, and further achievement of structural and functional parts. In the realm of ceramics, the following are the most promising methods:

- Vat photopolymerization produces parts with superior surface finish and resolution, but faces major, and yet unsolved, challenges for dark-colored ceramic materials with high absorbance and index of refraction difference from photocurable resins. For this reason, many advanced ceramics including carbides, borides, and nitrides have

experienced limited success in this technique. Industrial ceramic additive manufacturing is heavily focused on this technique, with oxide ceramics as the main feedstock material.

- Powder bed processes, binder jetting and powder bed fusion, have the benefit of supported overhang structures and wide material selections, but demonstrate poor surface finish and low green body density. Powder feedstocks for these processes are generally coarse in size to maintain free-flowing behavior. Conversely, the final properties of ceramic components rely heavily on fine microstructures and full density, which require the use of fine, often sub-micrometer, feedstock powders and high green body density [34]. This technique excels at producing scaffolds with high porosity for applications such as medical implants.
- Sheet lamination has the longest history to draw upon for insights and process optimization due to its beginnings from tape-casting in the 1940s. The tape-casting process is well understood and is currently automated and scaled for industrial use. If interfacial defects and delamination issues can be minimized, this is one of the most promising processes for manufacturing structural ceramic components and composites.
- Material extrusion processes enable a wide material selection and utilize low-cost equipment. Using two or more nozzles or a mixing head, composite parts can be produced with discrete and continuous composition variation. Feedstock material can be loaded to the highest ceramic content out of all AM families, enabling dense, structural components. The main drawbacks are poor resolution and surface finish.

The commercial ceramic AM sectors are focused on the above processes: vat photopolymerization, binder jetting, powder bed fusion, sheet lamination, and material extrusion. Most of the major commercial suppliers of ceramic AM equipment and parts utilize vat photopolymerization, including 3DCeram, Admatec, EnvisionTEC, Lithoz, and Tethon3D [156]. Admatec printers use a hybrid process between vat photopolymerization and sheet lamination, wherein a doctor blade is used to produce a uniform thickness layer of high ceramic-content photocurable slurry that is selectively cured using UV light. ExOne uses binder jetting to form green ceramic parts that are subsequently sintered, while II–VI MCubed uses binder jetting to print ceramic preforms followed by reaction bonding. Wuhan Binhu manufactures printers for PBF of ceramic materials. Helisys printers use the sheet lamination process and focus on creating composites. 3D Systems, Solidscape, Stratasys, and nScrypt produce material extrusion equipment focused on dental and bioprinting applications. Commercial suppliers support relatively few ceramic materials including alumina, zirconia, and silicon nitride, but are beginning to gain ground proving the industrial viability for these few optimized material systems.

10.2. Future directions

Although substantial progress has been made, challenges identified in initial research and during the inception of additive manufacturing processes still exist today. Challenges

include feedstock design, printing and post-processing related defects, process control and monitoring, and anisotropic mechanical properties [53]. To mature ceramic AM, each of these areas must be addressed.

Feedstock design challenges continue to hold back ceramic AM. Databases should be developed that contain the physical and chemical properties, optimal printing and post-processing parameters, resultant microstructural evolution, and application-based recommendations for ceramic feedstock materials. For example, a database could outline reactive processing relationships between various ceramic materials [157]. Reactive processing techniques such as reaction bonding [102] and melt infiltration [123] were discussed in this review, but were achieved during post-processing. A database of compatible feedstock materials would accelerate research into in-situ reactive processing for direct AM processes such as PBF [158], which show significant promise but need further development for industrial use. Similarly, a database of precursor materials for polymer-derived ceramics and their processing parameters could advance progress in that area. Schmidt et al. [159] demonstrated multi-scale ceramic lattice structures using a hybrid AM process combining DLP and two-photo lithography (2 PL). In this work, the PDC method enabled sub-micron features on centimeter-sized parts by removing the challenge of using sub-micron ceramic feedstock materials that can also be sintered to full density. Successful research into sub-micron ceramic feedstock materials that can be processed could enable a similar hybrid approach for bulk, structural ceramics.

In-situ monitoring of the printing process needs to be explored to improve quality control and control defects. Several monitoring techniques have been explored for polymer and metal AM processes, including nozzle pressure and temperature sensing [160] and melt-pool thermal analysis for metal PBF [161], but little work on in-situ monitoring and feedback control for ceramic AM processes exists. A process monitoring technique based on image signature analysis was developed to detect defects for FDC [162], but a feedback loop was not implemented and the system required manual calibration and image pre-processing. Implementing nozzle pressure sensors with feedback control for ceramic suspension extrusion processes would enable consistent trace width and improve part quality. Monitoring by X-ray computed tomography has the potential to detect voids in real-time, which could provide valuable feedback to optimize processing parameters and reduce printing derived defects.

Few direct processes have been explored due to the high processing temperature and brittle nature of ceramic materials. Future research should look in-depth at direct processes because much of the time and energy costs for ceramic AM stem from post-processing. Novel sintering methods such as flash and microwave sintering may offer opportunities to improve single-step ceramic AM processes. Recent work by the Kovar group at UT Austin [163] studied the use flash sintering for ceramic PBF with limited success due to thermal cracking and uneven initiation of flash. Improved process control will be necessary to push these novel methods forward.

Compared with the direct AM processes used for metals and polymers, indirect processing of ceramic materials is an

advantage when it comes to avoiding anisotropic mechanical properties. If printing defects can be eliminated, post-processing and densification should eliminate layer interfaces. Microstructure texturing that occurs in direct metal AM processes should not affect ceramic components, which are sintered in secondary steps. Through the use of composition gradients, sharp transitions in multi-material parts that lead to internal stress concentrations, cracking, and delamination at interfaces may be eliminated [49]. Material deposition processes, including material jetting, material extrusion, and directed energy deposition, are especially suited to multi-material fabrication as they are essentially one-dimensional processes where the feed can be adjusted at any voxel. Fabrication of functionally graded composites has the potential to greatly improve damage tolerance of ceramic materials, which are typically brittle with defect-dominated mechanical properties. Further, hierarchical design, following that of natural structures, should be explored through several levels of structuring: macro and meso-scale features can be produced by nozzle pathing; fiber and particle alignment at the microscale could be controlled with shear gradients from doctor blades used for tape casting and spreader blades for vat photopolymerization or pressure gradients in extrusion nozzles; nanoscale structures could be achieved by grain boundary additives.

Declaration of Competing Interest

The authors declare that they have no known competing financial interests or personal relationships that could have appeared to influence the work reported in this paper.

Acknowledgements

The authors would like to thank the members of the Ceramic and Transparent Materials Branch at the DEVCOM Army Research Laboratory, Aberdeen Proving Ground, MD. The authors want to acknowledge the members of the Meyers group at UCSD, for their help editing this review.

This research was sponsored by the DEVCOM Army Research Laboratory and was accomplished under Cooperative Agreement Number W911NF-19-2-0054. The views and conclusions contained in this document are those of the authors and should not be interpreted as representing the official policies, either expressed or implied, of the DEVCOM Army Research Laboratory or the U.S. Government. The U.S. Government is authorized to reproduce and distribute reprints for Government purposes notwithstanding any copyright notation herein.

REFERENCES

- [1] Arnold S, Coltman J. Design trade-offs for ceramic/composite armor materials. In: 22nd International SAMPE Technical Conference; 1990.
- [2] Bose S, Roy M, Bandyopadhyay A. Recent advances in bone tissue engineering scaffolds. *Trends Biotechnol* 2012;30(10). <https://doi.org/10.1016/j.tibtech.2012.07.005>.
- [3] Bose S, Ke D, Sahasrabudhe H, Bandyopadhyay A. Additive manufacturing of biomaterials. *Prog Mater Sci* 2018;93. <https://doi.org/10.1016/j.pmatsci.2017.08.003>.
- [4] Hwa LC, Rajoo S, Noor AM, Ahmad N, Uday MB. Recent advances in 3D printing of porous ceramics: a review. *Curr Opin Solid State Mater Sci* 2017;21:323–47. <https://doi.org/10.1016/j.cossms.2017.08.002>.
- [5] Chu TMG, Orton DG, Hollister SJ, Feinberg SE, Halloran JW. Mechanical and in vivo performance of hydroxyapatite implants with controlled architectures. *Biomaterials* 2002;23:1283–93. [https://doi.org/10.1016/S0142-9612\(01\)00243-5](https://doi.org/10.1016/S0142-9612(01)00243-5).
- [6] Bose S, Vahabzadeh S, Bandyopadhyay A. Bone tissue engineering using 3D printing. *Materials Today* 2013;16(12):496–504. <https://doi.org/10.1016/j.mattod.2013.11.017>.
- [7] Muth JT, Dixon PG, Woish L, Gibson LJ, Lewis JA. Architected cellular ceramics with tailored stiffness via direct foam writing. *Proc Natl Acad Sci* 2017;114:1832–7. <https://doi.org/10.1073/pnas.1616769114>.
- [8] Bae C, Halloran JW. Integrally cored ceramic investment casting mold fabricated by ceramic stereolithography. *Int J Appl Ceram Technol* 2008;8(6). <https://doi.org/10.1111/j.1744-7402.2010.02568.x>.
- [9] Weng F, Chen C, Yu H. Research status of laser cladding on titanium and its alloys: a review. *Mater Des* 2014;58. <https://doi.org/10.1016/j.matdes.2014.01.077>.
- [10] Zhang Y, Sahasrabudhe H, Bandyopadhyay A. Additive manufacturing of Ti-Si-N ceramic coatings on titanium. *Appl Surf Sci* 2015;346:428–37. <https://doi.org/10.1016/j.apsusc.2015.03.184>.
- [11] Balla VK, Bandyopadhyay PP, Bose S, Bandyopadhyay A. Compositionally graded yttria-stabilized zirconia coating on stainless steel using laser engineered net shaping (LENS™). *Scr Mater* 2007;57:861–4. <https://doi.org/10.1016/j.scriptamat.2007.06.055>.
- [12] Wang HM, Wang CM, Cai LX. Wear and corrosion resistance of laser clad Ni₂Si/NiSi composite coatings. *Surf Coatings Technol* 2003;168. [https://doi.org/10.1016/S0257-8972\(03\)00240-8](https://doi.org/10.1016/S0257-8972(03)00240-8).
- [13] Xu X, Han J, Wang C, Huang A. Laser cladding of composite bioceramic coatings on titanium alloy. *J Mater Eng Perform* 2016;25. <https://doi.org/10.1007/s11665-015-1868-4>.
- [14] Gao W, Zhang Y, Ramanujan D, Ramani K, Chen Y, Williams CB, et al. The status, challenges, and future of additive manufacturing in engineering. *CAD Comput Aided Des* 2015;69:65–89. <https://doi.org/10.1016/j.cad.2015.04.001>.
- [15] Carter CB, Norton MG. *Ceramic materials: science and engineering*. Springer; 2013.
- [16] Travitzky N, Bonet A, Dermeik B, Fey T, Filbert-Demut I, Schlier L, et al. Additive manufacturing of ceramic-based materials. *Adv Eng Mater* 2014;16:729–54. <https://doi.org/10.1002/adem.201400097>.
- [17] Richerson D, Lee W. *Applications and processing of ceramics*. *Mod Ceram Eng*. 2006.
- [18] Le Ferrand H. Magnetic slip casting for dense and textured ceramics: a review of current achievements and issues. *J Eur Ceram Soc* 2021;41(1). <https://doi.org/10.1016/j.jeurceramsoc.2020.08.030>.
- [19] Morissette SL, Lewis J a, Cesarano J, Dimos DB, Baer TY. Solid freeform fabrication of aqueous alumina-poly(vinyl alcohol) gelcasting suspensions. *J Am Ceram Soc* 2000;83:2409–16. <https://doi.org/10.1111/j.1151-2916.2000.tb01569.x>.

- [20] Yang J, Yu J, Huang Y. Recent developments in gelcasting of ceramics. *J Eur Ceram Soc* 2011;31. <https://doi.org/10.1016/j.jeurceramsoc.2010.12.035>.
- [21] Wiesner VL, Youngblood JP, Trice RW. Room-temperature injection molding of aqueous alumina-polyvinylpyrrolidone suspensions. *J Eur Ceram Soc* 2014;34:453–63. <https://doi.org/10.1016/j.jeurceramsoc.2013.08.017>.
- [22] Tariolle S, Reynaud C, Thévenot F, Chartier T, Besson JL. Preparation, microstructure and mechanical properties of SiC-SiC and B 4C-B4C laminates. *J Solid State Chem* 2004;177:487–92. <https://doi.org/10.1016/j.jssc.2003.02.007>.
- [23] Klocke F. Modern approaches for the production of ceramic components. *J Eur Ceram Soc* 1997;17(2):457–65. [https://doi.org/10.1016/s0955-2219\(96\)00163-x](https://doi.org/10.1016/s0955-2219(96)00163-x).
- [24] Griffith ML, Halloran JW. Freeform fabrication of ceramics via stereolithography. *J Am Ceram Soc* 1996;79(10):2601–8. <https://doi.org/10.1111/j.1151-2916.1996.tb09022.x>.
- [25] Peng E, Zhang D, Ding J. Ceramic robocasting: recent achievements, potential, and future developments. *Adv Mater* 2018;30:1–14. <https://doi.org/10.1002/adma.201802404>.
- [26] Oxman N, Keating S, Tsai E. Functionally graded rapid prototyping. *Innov Dev Virtual Phys Prototyp* 2012;483–9. <https://doi.org/10.1201/b11341-78>.
- [27] Wilkerson RP, Gludovatz B, Watts J, Tomsia AP, Hilmas GE, Ritchie RO. A study of size effects in bioinspired, “nacre-like”, metal-compliant-phase (nickel-alumina) coextruded ceramics. *Acta Mater* 2018;148:147–55. <https://doi.org/10.1016/j.actamat.2018.01.046>.
- [28] Pelz JS, Ku N, Shoulders WT, Meyers MA, Vargas-Gonzalez LR. Multi-material additive manufacturing of functionally graded carbide ceramics via active, in-line mixing. *Additive Manufacturing* 2020;37. <https://doi.org/10.1016/j.addma.2020.101647>.
- [29] 52900 :2015 A. Standard terminology for additive manufacturing – general principles – terminology. *ASTM Int*; 2015. p. 1–9. <https://doi.org/10.1520/F2792-12A.2>.
- [30] Jauhar S, Asthankar KM, Kuthe AM. Cost benefit analysis of rapid manufacturing in automotive industries. *Adv Mech Eng Appl* 2012:181–8.
- [31] Atzeni E, Salmi A. Economics of additive manufacturing for end-useable metal parts. *Int J Adv Manuf Technol* 2012;62:1147–55. <https://doi.org/10.1007/s00170-011-3878-1>.
- [32] Ngo TD, Kashani A, Imbalzano G, Nguyen KTQ, Hui D. Additive manufacturing (3D printing): a review of materials, methods, applications and challenges. *Compos Part B Eng* 2018;143:172–96. <https://doi.org/10.1016/j.compositesb.2018.02.012>.
- [33] Sachs E, Cima M, Cornie J. Three-dimensional printing: rapid tooling and prototypes directly from a CAD model. *CIRP Ann-Manuf Technol* 1990;39:201–4. [https://doi.org/10.1016/S0007-8506\(07\)61035-X](https://doi.org/10.1016/S0007-8506(07)61035-X).
- [34] Lewis JA. Colloidal processing of ceramics. *J Am Ceram Soc* 2000;83:2341–59. <https://doi.org/10.1111/j.1151-2916.2000.tb01560.x>.
- [35] Zocca A, Colombo P, Gomes CM, Günster J. Additive manufacturing of ceramics: issues, potentialities, and opportunities. *J Am Ceram Soc* 2015;98:1983–2001. <https://doi.org/10.1111/jace.13700>.
- [36] Krell A, Schädlich S. Nanoindentation hardness of submicrometer alumina ceramics. *Mater Sci Eng A* 2001;307. [https://doi.org/10.1016/S0921-5093\(00\)01818-9](https://doi.org/10.1016/S0921-5093(00)01818-9).
- [37] Yap CY, Chua CK, Dong ZL, Liu ZH, Zhang DQ, Loh LE, et al. Review of selective laser melting: materials and applications. *Appl Phys Rev* 2015;2. <https://doi.org/10.1063/1.4935926>.
- [38] Kodama H. JPS56144478A: stereoscopic figure drawing device. 1980.
- [39] Kodama Hideo. Automatic method for fabricating a three-dimensional plastic model with photo-hardening polymer. *Rev Sci Instrum* 1981;52.
- [40] Hull CW. Apparatus for production of three-dimensional objects by stereolithography. 4575330. 1984.
- [41] Gornet T, Wohlers T. History of additive manufacturing. *Wohlers Rep., Wohlers Report*. 2014. p. 1–34. <https://doi.org/10.1617/s11527-011-9818-6>.
- [42] Deckard CR, Beaman JJ, Darrah JF. Method for selective laser sintering with layerwise cross-scanning. 1986. <https://doi.org/US005485919A>.
- [43] Masters WE. US4665492A: computer automated manufacturing process and system. 1987. [https://doi.org/10.1016/0736-5845\(87\)90060-3](https://doi.org/10.1016/0736-5845(87)90060-3).
- [44] Feygin M. Apparatus and method for forming an integral object from laminations. US Pat 4752352. 1988.
- [45] Feygin M, Hsieh B. Laminated object manufacturing: a simpler process. In: *Proc 2nd solid Freeform Fabrication Symposium*; 1991. p. 123–30.
- [46] Crump SS. Apparatus and method for creating three-dimensional objects. 1989.
- [47] Sachs E, Haggerty J, Cima M, Williams P. Three-dimensional printing techniques. 1989. <https://doi.org/US005485919A>.
- [48] Kruth JP. Material increment manufacturing by rapid prototyping techniques. *CIRP Ann - Manuf Technol* 1991;40(2):603–14. [https://doi.org/10.1016/S0007-8506\(07\)61136-6](https://doi.org/10.1016/S0007-8506(07)61136-6).
- [49] Kruth JP, Leu MC, Nakagawa T. Progress in additive manufacturing and rapid prototyping. *CIRP Ann - Manuf Technol* 1998;47(2):525–40. [https://doi.org/10.1016/S0007-8506\(07\)63240-5](https://doi.org/10.1016/S0007-8506(07)63240-5).
- [50] Van der Schueren B, Geling J. Parts to go. *Prototyp Technol Int* 1998;48–52.
- [51] Rock SJ, Gilman CR. A new SFF process for functional Part Rapid prototyping and manufacturing: freeform powder molding. In: *Solid free fab symproc*; 1995. p. 80–7.
- [52] Wang JC, Dommati H, Hsieh SJ. Review of additive manufacturing methods for high-performance ceramic materials. *Int J Adv Manuf Technol* 2019;103. <https://doi.org/10.1007/s00170-019-03669-3>.
- [53] Allen AJ, Levin I, Witt SE. Materials research & measurement needs for ceramics additive manufacturing. *J Am Ceram Soc* 2020;103(11). <https://doi.org/10.1111/jace.17369>.
- [54] Halloran JW. Ceramic stereolithography: additive manufacturing for ceramics by photopolymerization. *Annu Rev Mater Res* 2016;46:19–40. <https://doi.org/10.1146/annurev-matsci-070115-031841>.
- [55] Griffith ML, Halloran JW. Stereolithography of ceramics. In: *Int sampe tech conf*, 27. 979: 970; 1995.
- [56] Griffith ML, Halloran JW. Ultraviolet curing of highly loaded ceramic suspensions for stereolithography of ceramics. In: *Solid free fab symproc*. University of Texas; 1994. p. 396–403.
- [57] Griffith ML, Halloran JW. Freeform fabrication of ceramics via stereolithography. *J Am Ceram Soc* 1996;79(10). <https://doi.org/10.1111/j.1151-2916.1996.tb09022.x>.
- [58] Griffith ML, Halloran JW. Scattering of ultraviolet radiation in turbid suspensions. *J Appl Phys* 1997;81. <https://doi.org/10.1063/1.364311>.
- [59] Garg R, Prud'homme RK, Aksay IA, Liu F, Alfano RR. Absorption length for photon propagation in highly dense colloidal dispersions. *J Mater Res* 1998;13:3463–7. <https://doi.org/10.1557/JMR.1998.0472>.
- [60] Hinczewski C, Corbel S, Chartier T. Ceramic suspensions suitable for stereolithography. *J Eur Ceram Soc* 1998;10(6). [https://doi.org/10.1016/s0955-2219\(97\)00186-6](https://doi.org/10.1016/s0955-2219(97)00186-6).

- [61] Chartier T, Chaput C, Doreau F, Loiseau M. Stereolithography of structural complex ceramic parts. *J Mater Sci* 2002;37. <https://doi.org/10.1023/A:1016102210277>.
- [62] Zhang K, He R, Ding G, Bai X, Fang D. Effects of fine grains and sintering additives on stereolithography additive manufactured Al₂O₃ ceramic. *Ceram Int* 2021;47:2303–10. <https://doi.org/10.1016/j.ceramint.2020.09.071>.
- [63] Zhang K, He R, Ding G, Feng C, Song W, Fang D. Digital light processing of 3Y-TZP strengthened ZrO₂ ceramics. *Mater Sci Eng A* 2020;774:138768. <https://doi.org/10.1016/j.msea.2019.138768>.
- [64] Schwentenwein M, Homa J. Additive manufacturing of dense alumina ceramics. *Int J Appl Ceram Technol* 2015;12(1). <https://doi.org/10.1111/ijac.12319>.
- [65] Scheithauer U, Schwarzer E, Moritz T, Michaelis A. Additive manufacturing of ceramic heat exchanger: opportunities and limits of the lithography-based ceramic manufacturing (LCM). *J Mater Eng Perform* 2018;27. <https://doi.org/10.1007/s11665-017-2843-z>.
- [66] Mitterramskogler G, Gmeiner R, Felzmann R, Gruber S, Hofstetter C, Stampfl J, et al. Light curing strategies for lithography-based additive manufacturing of customized ceramics. *Addit Manuf* 2014;1. <https://doi.org/10.1016/j.addma.2014.08.003>.
- [67] Ding G, He R, Zhang K, Xie C, Wang M, Yang Y, et al. Stereolithography-based additive manufacturing of gray-colored SiC ceramic green body. *J Am Ceram Soc* 2019;102. <https://doi.org/10.1111/jace.16648>.
- [68] Ding G, He R, Zhang K, Xia M, Feng C, Fang D. Dispersion and stability of SiC ceramic slurry for stereolithography. *Ceram Int* 2020;46:4720–9. <https://doi.org/10.1016/j.ceramint.2019.10.203>.
- [69] Ding G, He R, Zhang K, Zhou N, Xu H. Stereolithography 3D printing of SiC ceramic with potential for lightweight optical mirror. *Ceram Int* 2020;46:18785–90. <https://doi.org/10.1016/j.ceramint.2020.04.196>.
- [70] Zanchetta E, Cattaldo M, Franchin G, Schwentenwein M, Homa J, Brusatin G, et al. Stereolithography of SiOC ceramic microcomponents. *Adv Mater* 2016;28:370–6. <https://doi.org/10.1002/adma.201503470>.
- [71] Wang X, Schmidt F, Hanaor D, Kamm PH, Li S, Gurlo A. Additive manufacturing of ceramics from preceramic polymers: a versatile stereolithographic approach assisted by thiol-ene click chemistry. *Addit Manuf* 2019;27:80–90. <https://doi.org/10.1016/j.addma.2019.02.012>.
- [72] Colombo P, Mera G, Riedel R, Sorarù GD. Polymer-derived ceramics: 40 Years of research and innovation in advanced ceramics. *J Am Ceram Soc* 2010;93:1805–37. <https://doi.org/10.1111/j.1551-2916.2010.03876.x>.
- [73] Eckel ZC, Zhou C, Martin JH, Jacobsen AJ, Carter WB, Schaedler TA. Additive manufacturing of polymer-derived ceramics. *Sci Mag Res Rep* 2016;351:58–62.
- [74] O'Masta MR, Stonkevitch E, Porter KA, Bui PP, Eckel ZC, Schaedler TA. Additive manufacturing of polymer-derived ceramic matrix composites. *J Am Ceram Soc* 2020;103:6712–23. <https://doi.org/10.1111/jace.17275>.
- [75] Liu G, Zhao Y, Wu G, Lu J. Origami and 4D printing of elastomer-derived ceramic structures. *Sci Adv* 2018;4:1–11. <https://doi.org/10.1126/sciadv.aat0641>.
- [76] Chen H, Wang X, Xue F, Huang Y, Zhou K, Zhang D. 3D printing of SiC ceramic: direct ink writing with a solution of preceramic polymers. *J Eur Ceram Soc* 2018;38:5294–300. <https://doi.org/10.1016/j.jeurceramsoc.2018.08.009>.
- [77] Chen AN, Wu JM, Liu K, Chen JY, Xiao H, Chen P, et al. High-performance ceramic parts with complex shape prepared by selective laser sintering: a review. *Adv Appl Ceram* 2018;117:100–17. <https://doi.org/10.1080/17436753.2017.1379586>.
- [78] Subramanian K, Vail N, Barlow J, Marcus H. Selective laser sintering of alumina with polymer binders. *Rapid Prototyp J* 1995;1(2). <https://doi.org/10.1108/13552549510086844>.
- [79] Gähler A, Heinrich JG, Günster J. Direct laser sintering of Al₂O₃-SiO₂ dental ceramic components by layer-wise slurry deposition. *J Am Ceram Soc* 2006;89:3076–80. <https://doi.org/10.1111/j.1551-2916.2006.01217.x>.
- [80] Yves-Christian H, Jan W, Wilhelm M, Konrad W, Reinhart P. Net shaped high performance oxide ceramic parts by selective laser melting. *Phys Procedia* 2010;5:587–94. <https://doi.org/10.1016/j.phpro.2010.08.086>.
- [81] Wilkes J, Hagedorn YC, Meiners W, Wissenbach K. Additive manufacturing of ZrO₂-Al₂O₃ ceramic components by selective laser melting. *Rapid Prototyp J* 2013;19(1). <https://doi.org/10.1108/13552541311292736>.
- [82] Greulich M, Greul M, Pintat T. Fast, functional prototypes via multiphase jet solidification. *Rapid Prototyp J* 1995;1(1). <https://doi.org/10.1108/13552549510146649>.
- [83] Mapar M, Zhang DQ, Liu ZH, Yeong WY, Chua CK, Tay BY, et al. Preparation and flowability characterization of ceramic powders for selective laser melting. In: High value manuf. adv. res. virtual rapid prototyp. - proc. 6th int. conf. adv. res. rapid prototyping, VR@P 2013; 2014. <https://doi.org/10.1201/b15961-50>.
- [84] Lakshminarayan U, Ogrzydziak S, Marcus HL. Selective laser sintering of ceramic materials. In: *Int solid free fabr symp.* University of Texas; 1990. p. 16–26.
- [85] Vail NK, Barlow JW. Effect of polymer coatings as intermediate binders on sintering of ceramic parts. In: *Solid free fabr proc*; 1991. p. 195–204.
- [86] Nelson JC, Vail NK, Barlow JW. Laser sintering model for composite materials. In: *Solid free fabr symp*; 1993.
- [87] Christian Nelson J, Vail NK, Barlow JW, Beaman JJ, Bourell DL, Marcus HL. Selective laser sintering of polymer-coated silicon carbide powders. *Ind Eng Chem Res* 1995;34(5). <https://doi.org/10.1021/ie00044a017>.
- [88] Gureev DM, Ruzhechko RV, Shishkovskii IV. Selective laser sintering of PZT ceramic powders. *Tech Phys Lett* 2000;26. <https://doi.org/10.1134/1.1262811>.
- [89] Evans RS, Bourell DL, Beaman JJ, Campbell MI. Rapid manufacturing of silicon carbide composites. *Rapid Prototyping Journal* 2004;11(1):228–35.
- [90] Shahzad K, Deckers J, Kruth JP, Vleugels J. Additive manufacturing of alumina parts by indirect selective laser sintering and post processing. *J Mater Process Technol* 2013;213. <https://doi.org/10.1016/j.jmatprotec.2013.03.014>.
- [91] Liu K, Shi Y, Li C, Hao L, Liu J, Wei Q. Indirect selective laser sintering of epoxy resin-Al₂O₃ ceramic powders combined with cold isostatic pressing. *Ceram Int* 2014;40:7099–106. <https://doi.org/10.1016/j.ceramint.2013.12.043>.
- [92] Bertrand P, Bayle F, Combe C, Goeriot P, Smurov I. Ceramic components manufacturing by selective laser sintering. *Appl Surf Sci* 2007;254. <https://doi.org/10.1016/j.apsusc.2007.08.085>.
- [93] Hagedorn YC, Balachandran N, Meiners W, Wissenbach K, Poprawe R. SLM of net-shaped high strength ceramics: new opportunities for producing dental restorations. In: *22nd annu int solid free fabr symp - an addit manuf conf SFF*; 2011. p. 536–46.
- [94] Halloran JW. Freeform fabrication of ceramics. *Br Ceram Trans* 1999;98:299–303. <https://doi.org/10.1179/096797899680633>.
- [95] Fromm JE. Numerical calculation of the fluid dynamics of drop-on-demand jets. *IBM J Res Dev* 1984;28(3). <https://doi.org/10.1147/rd.283.0322>.
- [96] Sachs E, Cima M, Cornie J, Brancazio D, Bredt J, Curodeau A, et al. Three-dimensional printing: the physics and implications of additive manufacturing. *CIRP Ann - Manuf*

- Technol 1993;42(1). [https://doi.org/10.1016/S0007-8506\(07\)62438-X](https://doi.org/10.1016/S0007-8506(07)62438-X).
- [97] Butscher A, Bohner M, Doebelin N, Hofmann S, Müller R. New depowdering-friendly designs for three-dimensional printing of calcium phosphate bone substitutes. *Acta Biomater* 2013;9(11). <https://doi.org/10.1016/j.actbio.2013.07.019>.
- [98] Yoo J, Cho KM, Bae WS, Cima M, Suresh S. Transformation-toughened ceramic multilayers with compositional gradients. *J Am Ceram Soc* 1998;81(1). <https://doi.org/10.1111/j.1151-2916.1998.tb02291.x>.
- [99] Lanzetta M, Sachs E. Improved surface finish in 3D printing using bimodal powder distribution. *Rapid Prototyp J* 2003;9(3). <https://doi.org/10.1108/13552540310477463>.
- [100] Gonzalez JA, Mireles J, Lin Y, Wicker RB. Characterization of ceramic components fabricated using binder jetting additive manufacturing technology. *Ceram Int* 2016;42(9). <https://doi.org/10.1016/j.ceramint.2016.03.079>.
- [101] Kunchala P, Kappagantula K. 3D printing high density ceramics using binder jetting with nanoparticle densifiers. *Mater Des* 2018;155. <https://doi.org/10.1016/j.matdes.2018.06.009>.
- [102] Karandikar P, Watkins M, McCormick A, Givens B, Aghajanian M. Additive manufacturing (3D printing) of ceramics: microstructure, properties, and product examples. In: *Ceram Eng Sci Proc*. 38; 2018. p. 175–90. <https://doi.org/10.1002/9781119474746.ch17>.
- [103] Song JH, Edirisinghe MJ, Evans JRG. Formulation and multilayer jet printing of ceramic inks. *J Am Ceram Soc* 1999;82(12). <https://doi.org/10.1111/j.1151-2916.1999.tb02253.x>.
- [104] Blazdell PF, Evans JRG, Edirisinghe MJ, Shaw P, Binstead MJ. The computer aided manufacture of ceramics using multilayer jet printing. *J Mater Sci Lett* 1995;14. <https://doi.org/10.1007/BF00455415>.
- [105] Teng WD, Edirisinghe MJ. Development of ceramic inks for direct continuous jet printing. *J Am Ceram Soc* 1998;81(4). <https://doi.org/10.1111/j.1151-2916.1998.tb02443.x>.
- [106] Seerden KAM, Reis N, Evans JRG, Grant PS, Halloran JW, Derby B. Ink-jet printing of wax-based alumina suspensions. *J Am Ceram Soc* 2001;84(11). <https://doi.org/10.1111/j.1151-2916.2001.tb01045.x>.
- [107] Derby B, Reis N. Inkjet printing of highly loaded particulate suspensions. *MRS Bull* 2003;28. <https://doi.org/10.1557/mrs2003.230>.
- [108] Reis N, Ainsley C, Derby B. Ink-jet delivery of particle suspensions by piezoelectric droplet ejectors. *J Appl Phys* 2005;97. <https://doi.org/10.1063/1.1888026>.
- [109] Wang T, Derby B. Ink-jet printing and sintering of PZT. *J Am Ceram Soc* 2005;88(8). <https://doi.org/10.1111/j.1151-2916.2005.00406.x>.
- [110] Howatt GN, Breckenridge RG, Brownlow JM. Fabrication of thin ceramic sheets for capacitors. *J Am Ceram Soc* 1947;30:237–42.
- [111] Howatt GN. Method of producing high dielectric high insulation ceramic plates. 1952.
- [112] Rodriguez AR, Cronin J. Process for manufacturing multilayer ceramic capacitors. 1966.
- [113] Griffin C, Daufenbach J, McMillin S. Solid freeform fabrication of functional ceramic components using a laminated object manufacturing technique. In: *Solid free fab conf*; 1994. p. 17–25. <https://doi.org/10.1002/ana.23630>.
- [114] Griffin EA, Mumm DR, Marshall DB. Rapid prototyping of functional ceramic composites. *Am Ceram Soc Bull* 1996;75(7).
- [115] Klosterman D, Chartoff R, Priore B, Osborne N, Graves G, Lightman A, et al. Structural composites via laminated object manufacturing LOM. In: *Solid free fab symproc*; 1996.
- [116] Himmer T, Nakagawa T, Noguchi H. Stereolithography of ceramics. In: *Solid free fab symproc*. 42; 1997.
- [117] Klosterman D, Chartoff R, Graves G, Osborne N, Priore B. Interfacial characteristics of composites fabricated by laminated object manufacturing. *Compos Part A Appl Sci Manuf* 1998;29(9). [https://doi.org/10.1016/S1359-835X\(98\)00088-8](https://doi.org/10.1016/S1359-835X(98)00088-8).
- [118] Rodrigues SJ, Chartoff RP, Klosterman DA, Agarwala M, Hecht N. Solid freeform fabrication of functional silicon nitride ceramics by laminated object manufacturing. In: *Proc solid free fab symproc*; 2000.
- [119] Steinau M, Travitzky N, Zipperle T, Greil P. Functionally graded ceramics derived from preceramic polymers. *Ceram Trans* 2010. <https://doi.org/10.1002/9780470880630.ch8>.
- [120] Gomes CM, Rambo CR, De Oliveira APN, Hotza D, Gouvêa D, Travitzky N, et al. Colloidal processing of glass-ceramics for laminated object manufacturing. *J Am Ceram Soc* 2009;92. <https://doi.org/10.1111/j.1151-2916.2009.03035.x>.
- [121] Park J, Tari MJ, Hahn HT. Characterization of the laminated object manufacturing (LOM) process. *Rapid Prototyp J* 2000;6(1). <https://doi.org/10.1108/13552540010309868>.
- [122] Karunakaran KP, Dibbi S, Shanmuganathan PV, Raju DS, Kakaraparti S. Efficient stock cutting for laminated manufacturing. *CAD Comput Aided Des* 2002;34(4). [https://doi.org/10.1016/S0010-4485\(01\)00087-2](https://doi.org/10.1016/S0010-4485(01)00087-2).
- [123] Weisensel L, Travitzky N, Sieber H, Greil P. Laminated object manufacturing (LOM) of SiSiC composites. *Adv Eng Mater* 2004;6(11). <https://doi.org/10.1002/adem.200400112>.
- [124] Franks GV, Tallon C, Studart AR, Sesso ML, Leo S. Colloidal processing: enabling complex shaped ceramics with unique multiscale structures. *J Am Ceram Soc* 2017;100:458–90. <https://doi.org/10.1111/jace.14705>.
- [125] Lewis JA. Direct ink writing of 3D functional materials. *Adv Funct Mater* 2006;16:2193–204. <https://doi.org/10.1002/adfm.200600434>.
- [126] Rueschhoff LM. Novel ceramic near-net shaped processing. 2017.
- [127] Agarwala MK, Bandyopadhyay A, van Weeren R, Safari A, Danforth SC, Langrana NA, et al. Fused deposition of ceramics: rapid fabrication of structural ceramic components. *Am Ceram Soc Bull* 1996;11:60–5.
- [128] Agarwala MK, Bandyopadhyay A, Van Weeren R. Fused deposition of ceramics (FDC) for structural silicon nitride components. In: *Proc solid free fab symproc*; 1996.
- [129] Agarwala MK, Jamalabad VR, Langrana NA, Safari A, Whalen PJ, Danforth SC. Structural quality of parts processed by fused deposition. *Rapid Prototyp J* 1996;2. <https://doi.org/10.1108/13552549610732034>.
- [130] Kupp D, Eifert H, Greul M, Kunstner M. Rapid prototyping of functional metal and ceramic components by the multiphase jet solidification (MSJ) process. In: *Proc solid free fab symproc*; 1997.
- [131] Cesarano J, Robocasting Grieco S. A new technique for the freeform fabrication of near-net-shape ceramics. *Mater Technol* 1997;12(3). <https://doi.org/10.1080/10667857.1997.11752736>.
- [132] Cesarano III J, Aksay IA, Bleier A. Stability of aqueous Al_2O_3 suspensions with poly(methacrylic acid) polyelectrolyte. *J Am Ceram Soc* 1988;71:250–5.
- [133] Baer TA, Cesarano III J, Calvert P. Recent developments in freeform fabrication of dense ceramics from slurry deposition. In: *Solid free fab proceedings*; Sept 1997.
- [134] Jafari MA, Han W, Mohammadi F, Safari A, Danforth SC, Langrana N. A novel system for fused deposition of advanced multiple ceramics. *Rapid Prototyp J* 2000;6(3). <https://doi.org/10.1108/13552540010337047>.

- [135] Smay JE, Nadkarni SS, Xu J. Direct writing of dielectric ceramics and base metal electrodes. *Int J Appl Ceram Technol* 2007;4:47–52. <https://doi.org/10.1111/j.1744-7402.2007.02118.x>.
- [136] Iyer S, Mcintosh J, Bandyopadhyay A, Langrana N, Safari A, Danforth SC, et al. Microstructural characterization and mechanical properties of Si_3N_4 formed by fused deposition of ceramics. *Int J Appl Ceram Technol* 2008;5:127–37. <https://doi.org/10.1111/j.1744-7402.2008.02193.x>.
- [137] Rueschhoff L, Costakis W, Michie M, Youngblood J, Trice R. Additive manufacturing of dense ceramic parts via direct ink writing of aqueous alumina suspensions. *Int J Appl Ceram Technol* 2016;13:821–30. <https://doi.org/10.1111/ijac.12557>.
- [138] Costakis WJ, Rueschhoff LM, Diaz-Cano AI, Youngblood JP, Trice RW. Additive manufacturing of boron carbide via continuous filament direct ink writing of aqueous ceramic suspensions. *J Eur Ceram Soc* 2016;36:3249–56. <https://doi.org/10.1016/j.jeurceramsoc.2016.06.002>.
- [139] Eqtesadi S, Motealleh A, Perera FH, Miranda P, Pajares A, Wendelbo R, et al. Fabricating geometrically-complex B4C ceramic components by robocasting and pressureless spark plasma sintering. *Scr Mater* 2018;145:14–8. <https://doi.org/10.1016/j.scriptamat.2017.10.001>.
- [140] Allahverdi M, Danforth SC, Jafari M, Safari A. Processing of advanced electroceramic components by fused deposition technique. *J Eur Ceram Soc* 2001;21(10). [https://doi.org/10.1016/S0955-2219\(01\)00047-4](https://doi.org/10.1016/S0955-2219(01)00047-4).
- [141] Franchin G, Wahl L, Colombo P. Direct ink writing of ceramic matrix composite structures. *J Am Ceram Soc* 2017;100:4397–401. <https://doi.org/10.1111/jace.15045>.
- [142] Feilden E, Ferraro C, Zhang Q, García-Tuñón E, D'Elia E, Giuliani F, et al. 3D printing bioinspired ceramic composites. *Sci Rep* 2017;7. <https://doi.org/10.1038/s41598-017-14236-9>.
- [143] Croom BP, Abbott A, Kemp JW, Rueschhoff L, Smieska L, Woll A, et al. Mechanics of nozzle clogging during direct ink writing of fiber-reinforced composites. *Addit Manuf* 2021;37:101701. <https://doi.org/10.1016/j.addma.2020.101701>.
- [144] Kemp JW, Diaz AA, Malek EC, Croom BP, Apostolov ZD, Kalidindi SR, et al. Direct ink writing of ZrB₂-SiC chopped fiber ceramic composites. *Addit Manuf* 2021;44:102049. <https://doi.org/10.1016/j.addma.2021.102049>.
- [145] Balla VK, Bose S, Bandyopadhyay A. Processing of bulk alumina ceramics using laser engineered net shaping. *Int J Appl Ceram Technol* 2008;5(3). <https://doi.org/10.1111/j.1744-7402.2008.02202.x>.
- [146] Niu F, Wu D, Ma G, Zhou S, Zhang B. Effect of second-phase doping on laser deposited Al_2O_3 ceramics. *Rapid Prototyp J* 2015;21(2). <https://doi.org/10.1108/RPJ-12-2014-0167>.
- [147] Tompkins JV, Laabi R, Birmingham BR, Marcus HL. Advances in selective area laser deposition of silicon carbide. In: *Solid free fabr symp*; 1994.
- [148] Jakubenas KJ, Lee YL, Shaarawi MS, Marcus HL, Sanchez JM. Selective area laser deposition of titanium oxide. *Rapid Prototyp J* 1997;3(2). <https://doi.org/10.1108/13552549710176699>.
- [149] Fessler J, Nickel a, Link G. Functional gradient metallic prototypes through shape deposition manufacturing. In: *Proc solid free fabr symp*; 1997. p. 521–8.
- [150] Crocker JE, Sun LC, Ansquer H, Shaw LL, Marcus HL. Processing and characterization of SALDVI ceramic structures. In: *Solid free fabr proceedings*; August 1999.
- [151] Niu F, Wu D, Ma G, Wang J, Guo M, Zhang B. Nanosized microstructure of Al_2O_3 -ZrO₂ (Y_2O_3) eutectics fabricated by laser engineered net shaping. *Scr Mater* 2015;95. <https://doi.org/10.1016/j.scriptamat.2014.09.026>.
- [152] Hu Y, Wang H, Cong W, Zhao B. Directed energy deposition of zirconia-toughened alumina ceramic: novel microstructure formation and mechanical performance. *J Manuf Sci Eng* 2020;142(2). <https://doi.org/10.1115/1.4045626>.
- [153] Hu Y, Ning F, Cong W, Li Y, Wang X, Wang H. Ultrasonic vibration-assisted laser engineering net shaping of ZrO_2 - Al_2O_3 bulk parts: effects on crack suppression, microstructure, and mechanical properties. *Ceram Int* 2018;44. <https://doi.org/10.1016/j.ceramint.2017.11.013>.
- [154] Liu Z, Ning F, Cong W, Jiang Q, Li T, Zhang H, et al. Energy consumption and saving analysis for laser engineered net shaping of metal powders. *Energies* 2016;9. <https://doi.org/10.3390/en9100763>.
- [155] Yan S, Wu D, Niu F, Ma G, Kang R. Al_2O_3 - ZrO_2 eutectic ceramic via ultrasonic-assisted laser engineered net shaping. *Ceram Int* 2017;43. <https://doi.org/10.1016/j.ceramint.2017.08.165>.
- [156] Golt M, Vargas-Gonzalez LR, Sietins J, Moorehead C, Blair V. *Additive manufacturing in ceramics: current status, capability gaps, and paths forward*. 2018.
- [157] Fahrenholtz WG. Reactive processing in ceramic-based systems. *Int J Appl Ceram Technol* 2006;3. <https://doi.org/10.1111/j.1744-7402.2006.02059.x>.
- [158] Peters AB, Zhang D, Hernandez A, Brupbacher MC, Nagle DC, Mueller T, et al. Selective laser sintering in reactive atmospheres: towards in-situ synthesis of net-shaped carbide and nitride ceramics. *Addit Manuf* 2021;45:102052. <https://doi.org/10.1016/j.addma.2021.102052>.
- [159] Schmidt J, Brigo L, Gandin A, Schwentenwein M, Colombo P, Brusatin G. Multiscale ceramic components from preceramic polymers by hybridization of vat polymerization-based technologies. *Addit Manuf* 2019;30:100913. <https://doi.org/10.1016/j.addma.2019.100913>.
- [160] Anderegg DA, Bryant HA, Ruffin DC, Skrip SM, Fallon JJ, Gilmer EL, et al. In-situ monitoring of polymer flow temperature and pressure in extrusion based additive manufacturing. *Addit Manuf* 2019;26. <https://doi.org/10.1016/j.addma.2019.01.002>.
- [161] Clijsters S, Craeghs T, Buls S, Kempen K, Kruth JP. In situ quality control of the selective laser melting process using a high-speed, real-time melt pool monitoring system. *Int J Adv Manuf Technol* 2014;75:1089–101. <https://doi.org/10.1007/s00170-014-6214-8>.
- [162] Fang T, Jafari MA, Danforth SC, Safari A. Signature analysis and defect detection in layered manufacturing of ceramic sensors and actuators. *Mach Vis Appl* 2003;15. <https://doi.org/10.1007/s00138-002-0074-1>.
- [163] Hagen D, Beaman JJ, Kovar D. Selective laser flash sintering of 8-YSZ. *J Am Ceram Soc* 2020;103:800–8. <https://doi.org/10.1111/jace.16771>.



Joshua Pelz has a BS in Metallurgical and Materials Engineering (2017) from the Colorado School of Mines and a MS in Material Science and Engineering (2019) from the University of California, San Diego. Currently, he is pursuing a Ph.D. in Material Science and Engineering at the University of California, San Diego. His Ph.D. research focuses on the development of custom additive manufacturing systems to generate functionally graded materials (polymeric and ceramic) for structural applications. Joshua is passionate about creative design and the use of advanced manufacturing

techniques to realize technological breakthroughs. His expertise in additive manufacturing techniques combined with a multi-disciplinary skill set covering mechanical, electrical, and software engineering provides a unique opportunity to solve cutting-edge problems. He designed a custom 3D printer that enables multi-material printing of advanced ceramics, which is in use at the UC San Diego, US Army Research Laboratory, Aberdeen, Westpoint Military Academy, and University of Delaware.



Dr. Nicholas Ku is a materials engineer at U.S. Army Combat Capabilities Development Command (DEVCOM) Army Research Laboratory within the Ceramics and Transparent Materials Branch. He received his PhD from the Materials Science and Engineering Department at Rutgers University in May 2015 for work in the area of fine particle cohesion and granulation. He also spent time at the University of Leeds as a visiting researcher conducting research on powder

flowability. Dr. Ku was then hired as a postdoctoral researcher at CCDC-ARL in July 2015, working in the area of particle synthesis and colloidal processing of nanocomposites. After being converted to a civilian employee in May 2018, Dr. Ku became the technical lead in ceramic additive manufacturing research within the Ceramics and Transparent Materials Branch. His current research areas include direct-ink write, vat polymerization, and binder jet manufacturing, as well as powder/colloidal processing and particulate suspension rheology. He has authored or co-authored multiple publications and technical reports, as well as a pending US patent.



Marc A. Meyers is Distinguished Professor of Materials Science at the University of California, San Diego. His research field is the mechanical behavior of materials. Within this field, he has focused on three areas: dynamic behavior of materials, nanocrystalline materials, and biological materials. In the dynamic behavior of materials, the unifying theme is the high rate at which events occur. He initiated this work in 1972 and has dedicated forty-five uninterrupted

years to it, unifying it by emphasizing the fundamental physical and chemical phenomena. This has been defined in his now classic book, *Dynamic Behavior of Materials* (1994, ~3,800 citations

in google scholar). He is the co-author of *Mechanical Metallurgy*, *Mechanical Behavior of Materials*, *Biological Materials Science* (CUP, 2014), and approximately 490 papers. His honors include Fellow, TMS, APS, ASM, and Explorers Club as well as awards in the US (APS Duvall, ASM Albert White, Charles Barrett (Rocky Mountain), and Sauveur, TMS Leadership, Cohen and Educator, Acta Materialia Materials and Society, MSEA Journal, SMD/TMS Distinguished Engineer/Scientist and Service), Europe (Luxembourg Grand Prix en Sciences, German Humboldt, DGM Heyn, and French DYMAT Rinehart), and China (Lee Hsun). He was co-founder of the Center for Explosives Technology Research, New Mexico Tech, and of the EXPLOMET conference series (1980-2000), as well as Associate Director and Director of the UCSD Institute for Mechanics and Materials, where he co-organized four summer schools. He co-chaired the first three Pan American Materials Conferences, which he co-founded. He is corresponding member of the Brazilian Academy of Sciences and of the Institut Grand Ducal (Luxembourg). He recently completed the Roosevelt-Rondon Centennial Expedition in honor of these two heroes.



Dr. Lionel Vargas-Gonzalez is a materials engineer for the U.S. Army Combat Capabilities Development Command (DEVCOM) Army Research Laboratory, currently serving as Chief (A) of the Ceramics and Transparent Materials Branch. He is a subject matter expert for materials manufacturing and processing science for dismounted Soldier protection. In his tenure at ARL, his research efforts have included synthesis and processing of lightweight Soldier materials (ceramics, ultra-high

molecular weight polyethylene), surface science and adhesion of dissimilar materials, and processing and manufacturing science efforts for improving ballistic mass efficiency and mitigation of physiological trauma effects in Soldier head and torso protection technologies. He is a co-recipient of the 2013 DoD ManTech Defense Manufacturing Achievement Award for development of lightweight body armor concepts, and the recipient of the 2015 ARL Honorary Award for Engineering for demonstration of composite architectural design for reduction of non-penetrating ballistic trauma. He is an author on over 50 publications, proceedings, and reports, and holds one U.S. Patent on processing of silicon carbide armor ceramics. He received a B.S. in Ceramic and Materials Engineering in 2004 from Clemson University, and a Ph.D. in Materials Science and Engineering in 2009 from the Georgia Institute of Technology.